7

Domain walls

Magnetization reversal in thin films and some relevant experimental methods

Maciej Urbaniak

Today's plan

- Domain walls in bulk materials
- Domain walls in thin films
- Domain walls in 1D systems
- Landau-Lifshitz-Gilbert equation – magnetization dynamics

Bloch versus Néel wall

•From previous lectures we know **Bloch** and Néel domain walls.

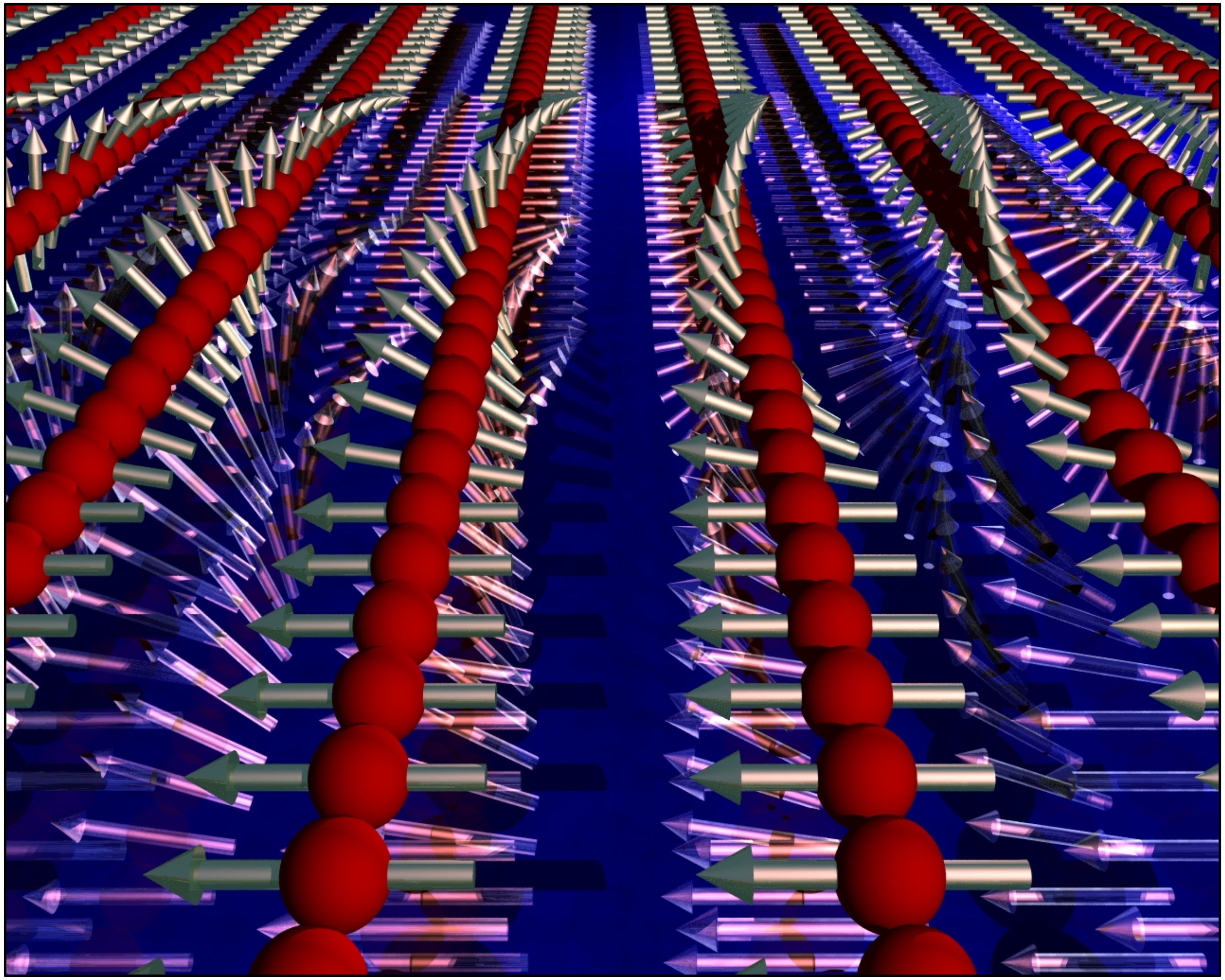

•Schematic view of the magnetic moments orientation of the Bloch wall in easy plane anisotropy sample
•The magnetic moments rotate gradually about the axis perpendicular to the wall

Bloch versus Néel wall

•From previous lectures we know **Bloch** and Néel domain walls.

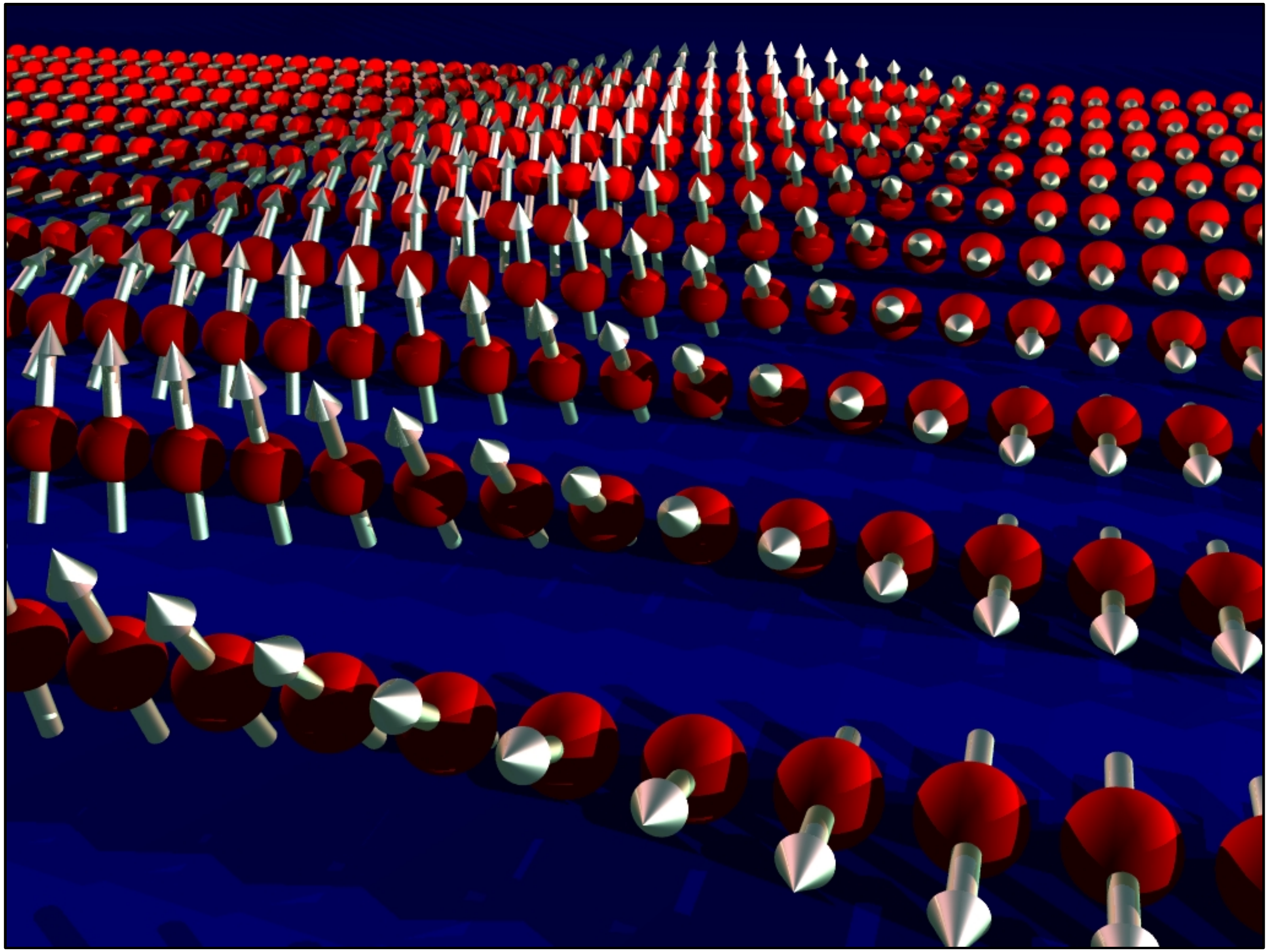

•To note is that when the Bloch wall in easy plane anisotropy sample crosses the surface of the sample the magnetic moments within the wall are **not parallel** to the surface

•**Magnetic charges** appear on the surface

Bloch versus Néel wall

•From previous lectures we know Bloch and **Néel** domain walls.

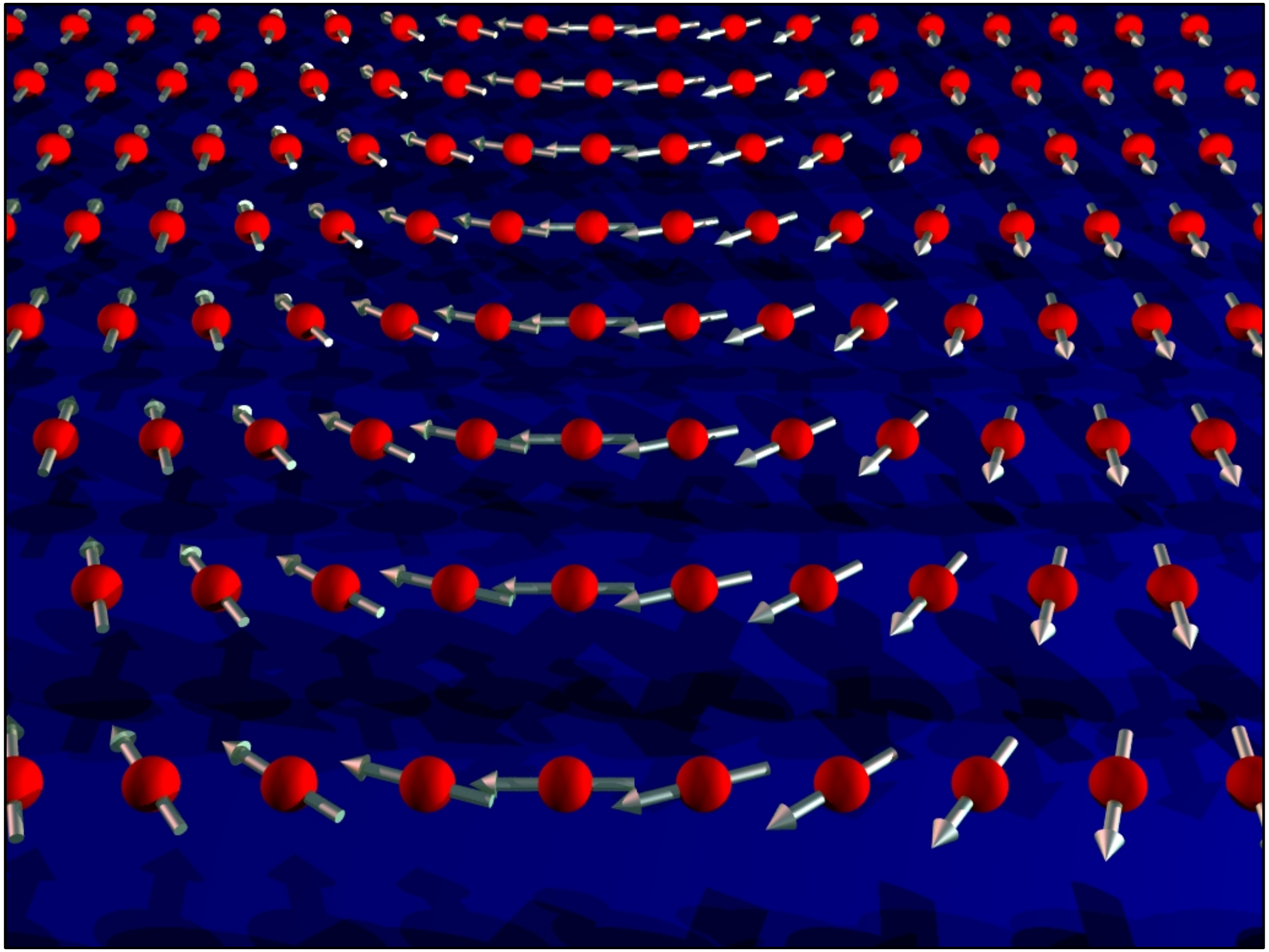

•Schematic view of the Néel wall
•Magnetic moments within Néel wall rotate along direction parallel to the wall
•To note is that when the Néel wall in easy plane anisotropy sample crosses the surface of the sample the magnetic moments within the wall are **parallel** to the surface

Bloch versus Néel wall

- The rotation of magnetic moments within the Néel wall creates volume magnetic charges.
- Assuming the following orientation of magnetization within Néel wall*:

$$\theta_{x\ axis}=\arctan(x); \qquad M_x=\cos(\theta_{x\ axis}) \qquad M_y=\sin(\theta_{x\ axis}) \qquad M_z=0$$

we obtain for the volume charge of the wall:

$$\rho_{magn}=-\nabla\cdot\vec{M}=-\left(\frac{\partial}{\partial x}M_x+\frac{\partial}{\partial y}M_y\right)=\frac{x}{(1+x^2)^{3/2}}$$

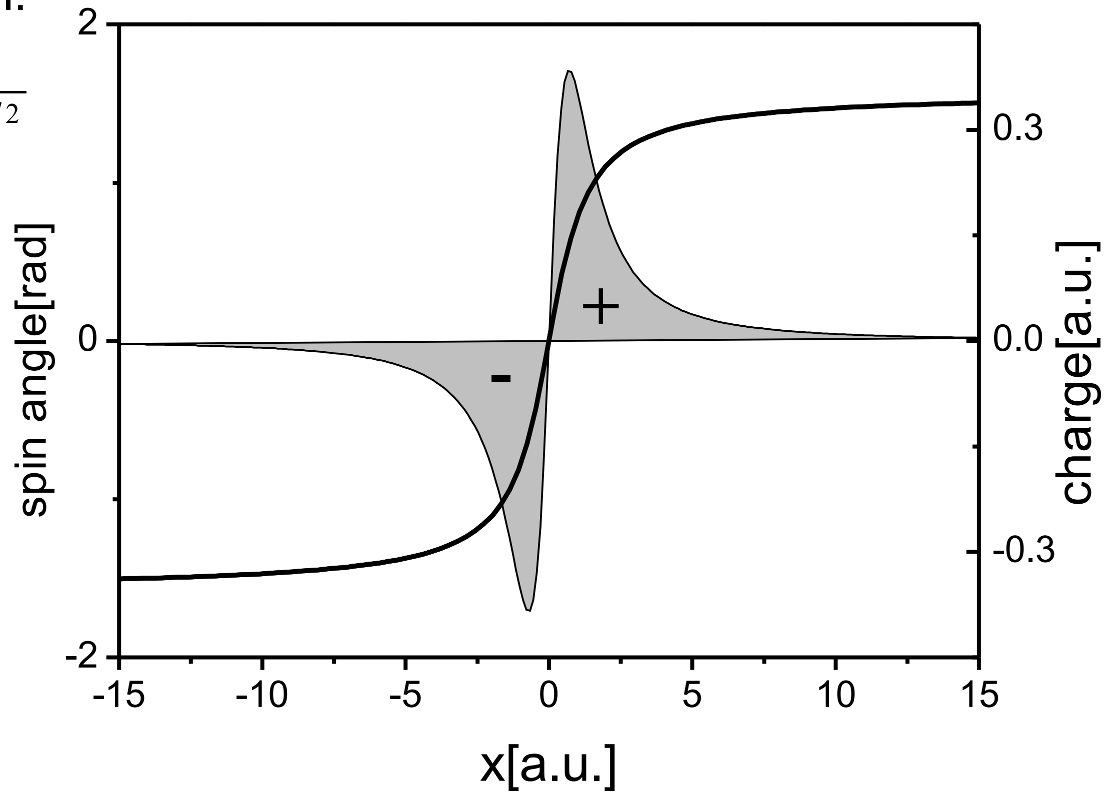

- Néel wall creates volume magnetic charges of opposite signs
- Néel wall, contrary to Bloch wall, is a source of magnetic field in infinite crystal
- Néel wall corresponds to a line of magnetic dipoles

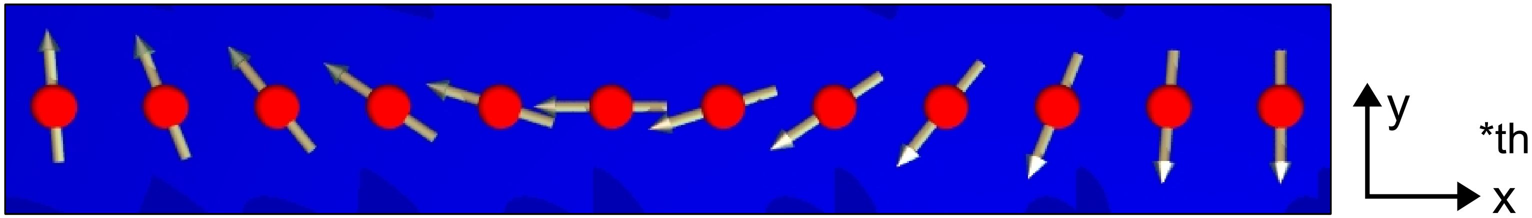

*this is just an approximation of the actual wall profile

Bloch wall in material with higher order anisotropy

- In uniaxial anisotropy material the energy is given by:

$$E_u = K_1 \sin^2\phi + K_2 \sin^4\phi$$

- In the previous derivation of the Bloch wall profile we have neglected the second order anisotropy constant K_2. It can be shown [1] that the wall profile with $K_2 \neq 0$ is given by:

$$\tan\phi = \sqrt{1+\kappa}\,\sinh\left(\frac{x}{\sqrt{A/K_1}}\right)$$

$$\kappa = K_2 / K_1$$

- Parameter κ must be larger than -1, otherwise the two domains are not stable [1]*.
- On approaching κ=-1 the wall divides into **two 90°**-walls which may, if the effective anisotropy is modified, split into two creating new domain.
- Widened walls are common in cubic anisotropy materials.

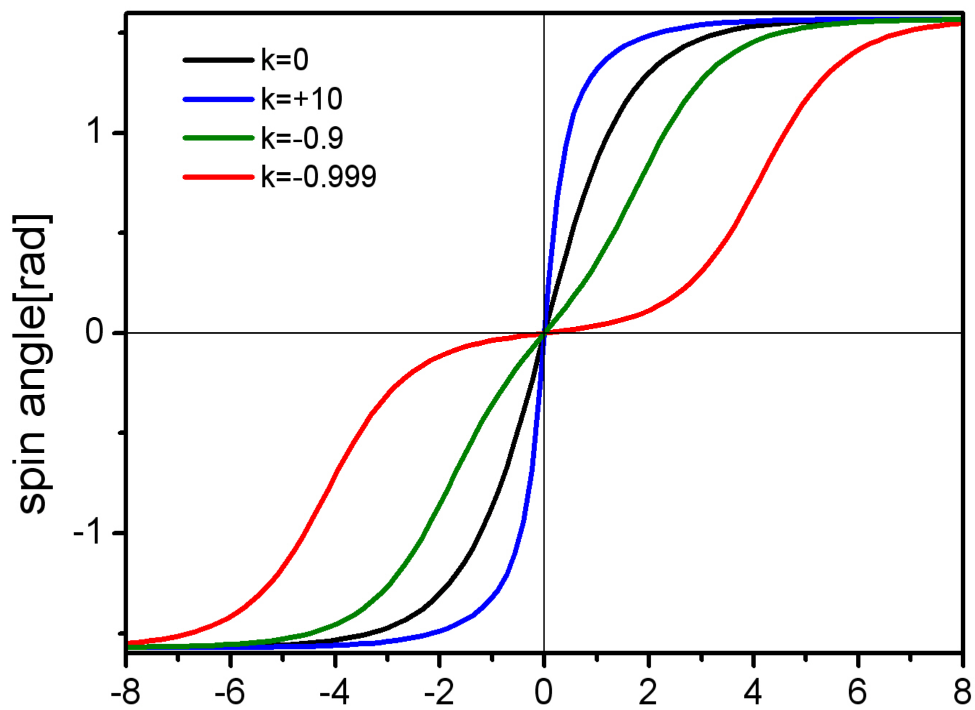

$$\frac{x}{\sqrt{A/K_1}}$$

*the magnetization with spin angle 0 would have lower energy than for ±π/2

graphics based on Fig.3.60 from [1]: A. Hubert, R. Schäfer, Magnetic domains: the analysis of magnetic microstructures, Springer 1998

Bloch wall in material with higher order anisotropy

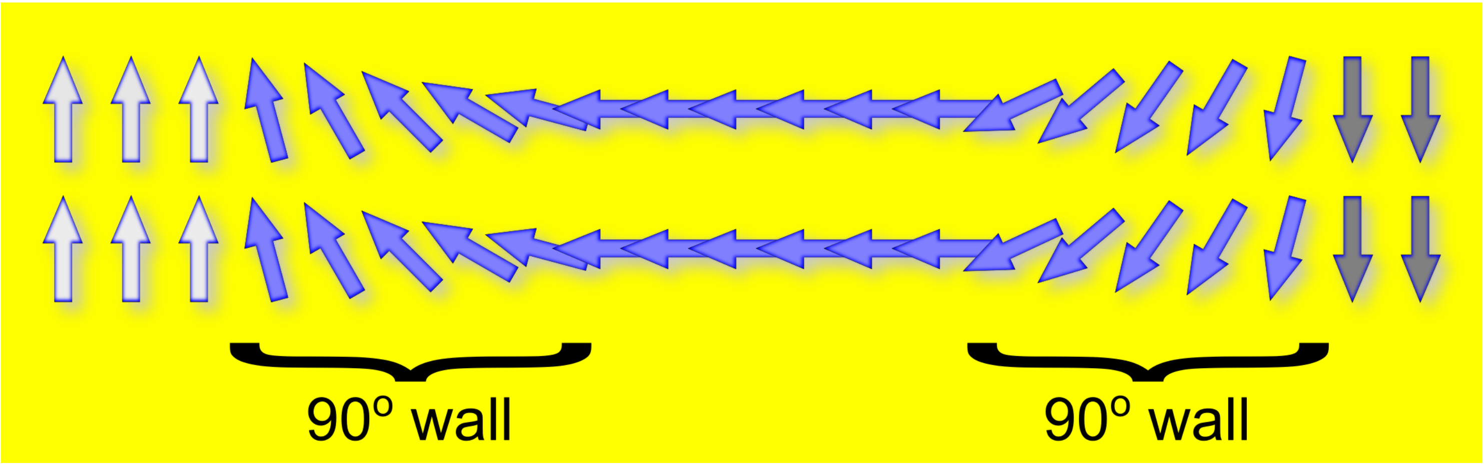

•Parameter κ must be larger than -1, otherwise the two domains are not stable [1]*.

•On approaching κ=-1 the wall divides into **two 90°**-walls which may, if the effective anisotropy is modified, split into two creating new domain.

•Widened walls are common in cubic anisotropy materials.

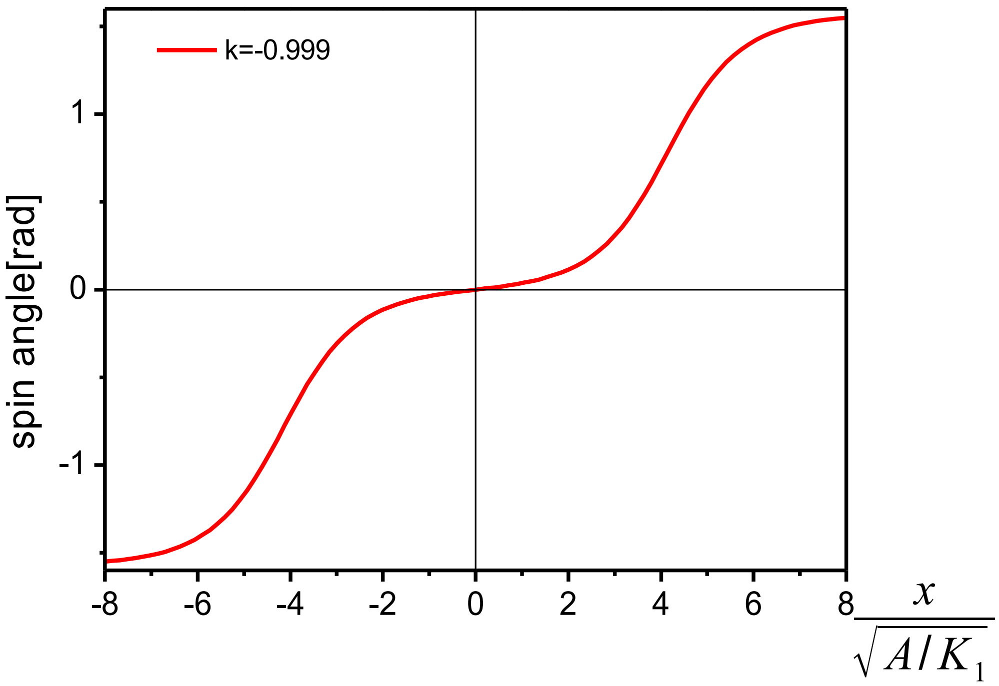

graphics based on Fig.3.60 from [1]: A. Hubert, R. Schäfer, Magnetic domains: the analysis of magnetic microstructures, Springer 1998

Bloch wall in material with higher order anisotropy

- Peculiarities of the wall profile influences the evaluation of wall width [1].
- For κ<-0.5 the wall profile has three points of inflection and the width is defined with the tangents in the outer inflection points (●).
- For other cases the thickness is defined as previously.

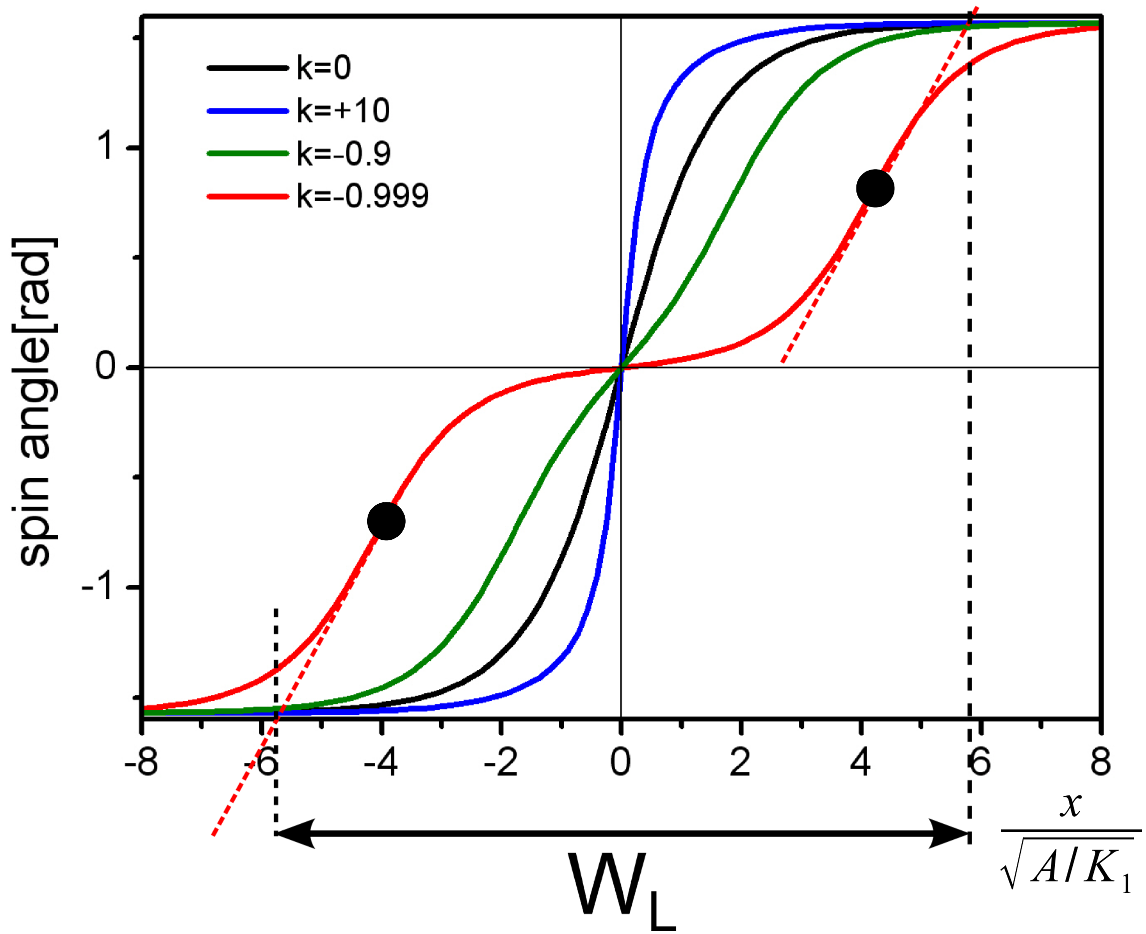

graphics based on Fig.3.60 from [1]: A. Hubert, R. Schäfer, Magnetic domains: the analysis of magnetic microstructures, Springer 1998

Domain walls in cubic anisotropy crystals

•In contrast to previously analyzed uniaxial anisotropy materials cubic anisotropy results in 3 or 4 easy axes (6 or 8 easy orientations of magnetization)
•In positive anisotropy crystals the preferred orientations are along <100> directions
•In negative anisotropy crystals the preferred orientations are along <111> directions

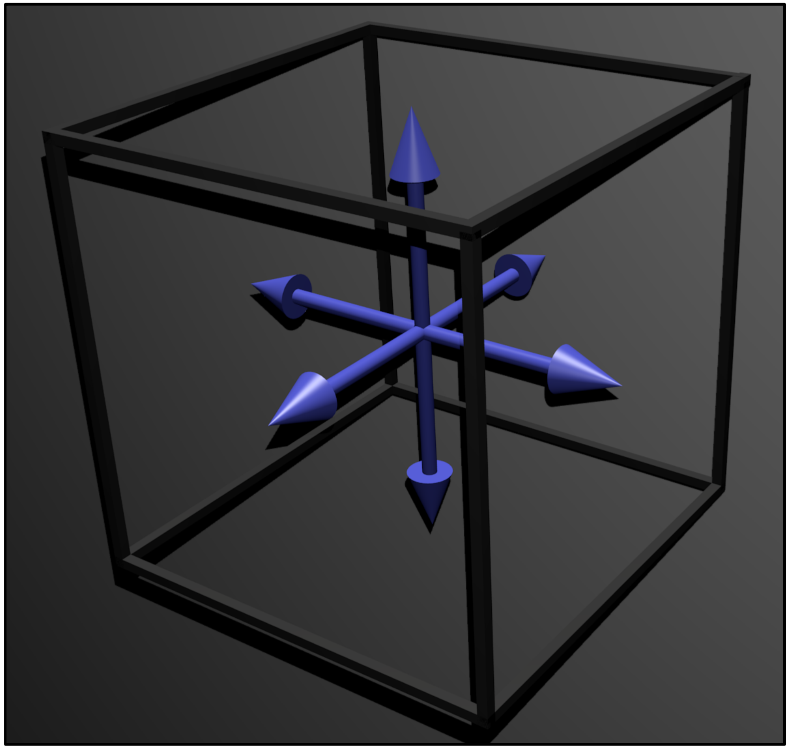

Preferred magnetization orientations
in Fe bulk crystals*
3 easy axes

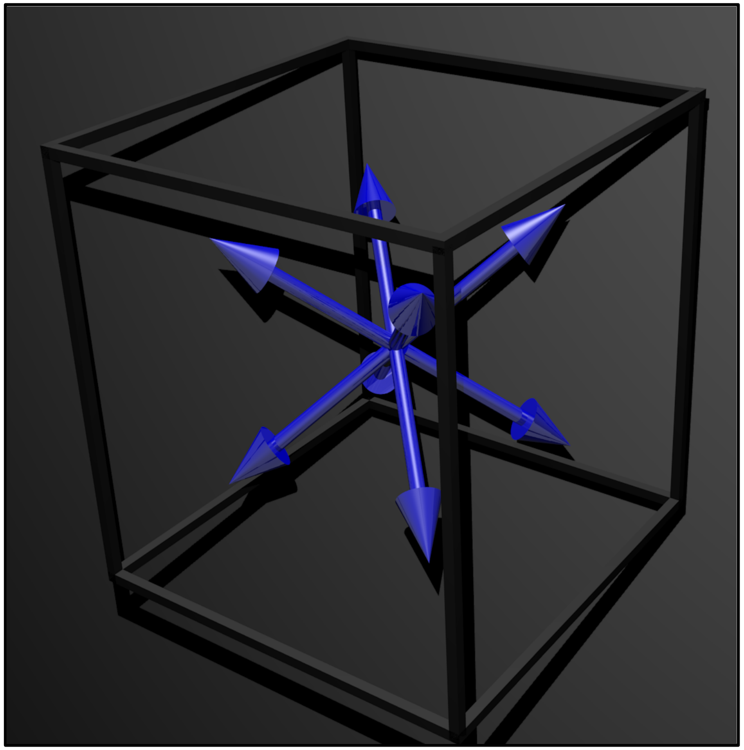

Preferred magnetization orientations
in Ni bulk crystals
4 easy axes

*without stress, external field etc.

Domain walls in cubic anisotropy crystals

•In positive anisotropy crystals the possible angles between unperturbed domain magnetizations are 90° and 180°
•In negative anisotropy crystals the allowable angles are 71° and 109°:

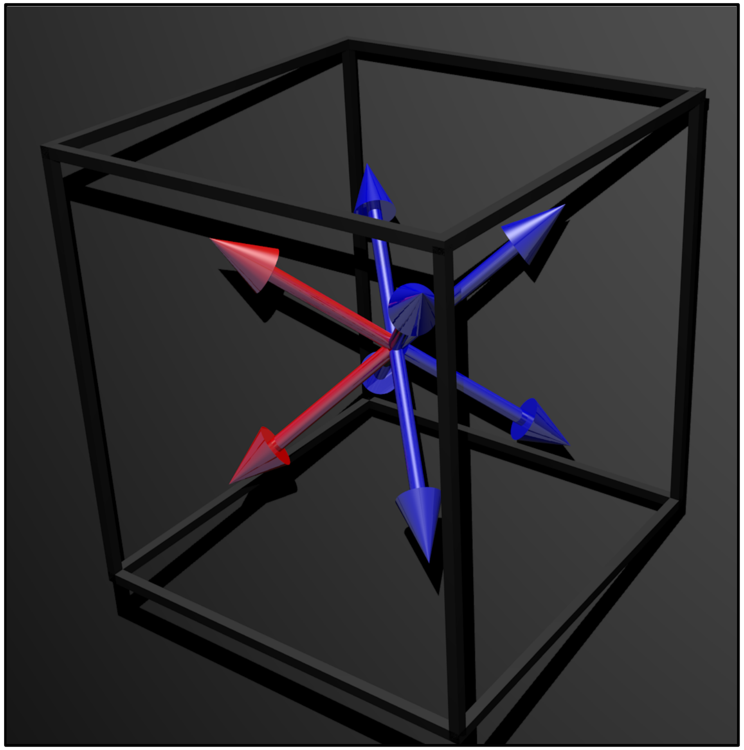

70.528°

109.472°

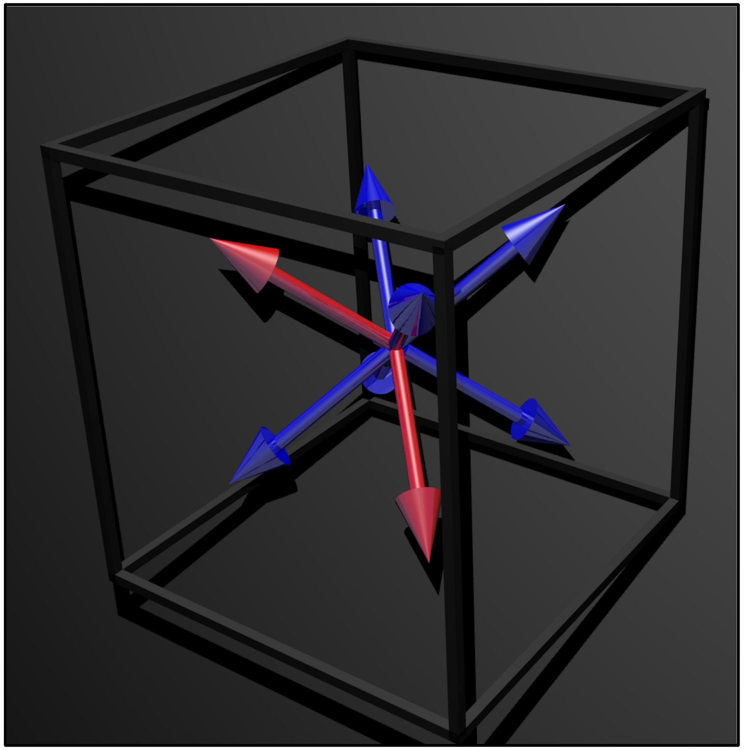

Preferred magnetization orientations
in Ni bulk crystals
4 easy axes

*without stress, external field etc.

Domain walls in cubic anisotropy crystals

•Due to anisotropy the energy of the domain wall depends on its orientation relative to the crystal axes:

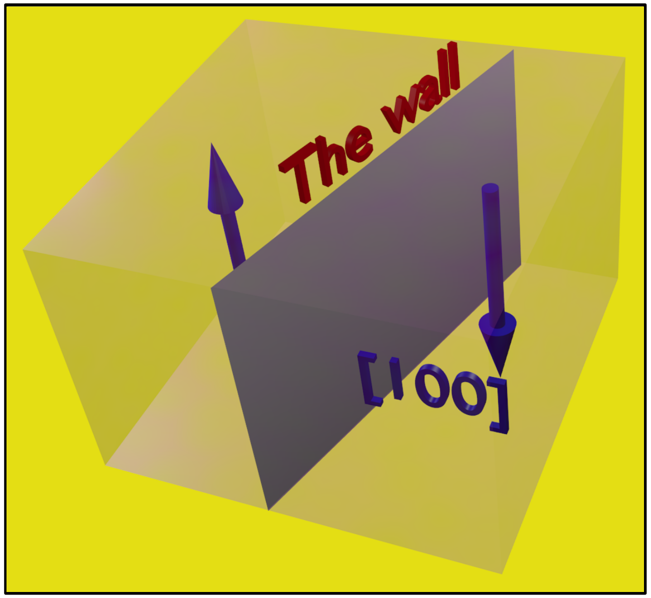

•Magnetostaic energy does not restrict the orientation of domain wall
•We assume the magnetization direction to rotate from [100] to its opposite direction
•In static equilibrium no field can exist in cubic material with 180^o wall [1]:
-the field parallel to [100] direction would force the wall to move as in uniaxial crystals
-the field component within the (100) plane would favour other domains

The preferred orientation of 180^o wall in (100) oriented transformer steel favours wall shapes as shown, in contrast to straight, perpendicular walls (image from A. Hubert [1] - Fig. 3.64)

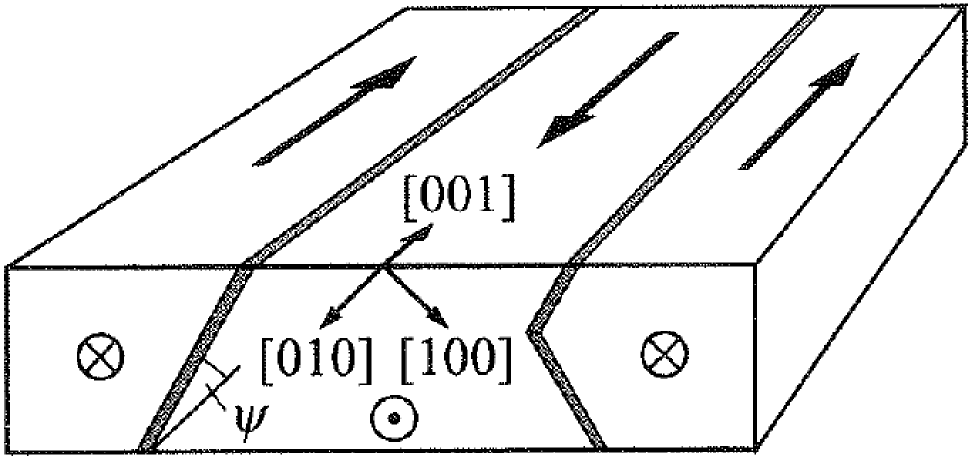

Domain walls in thin films

•Magnetic films are defined as **thin** if their thickness is comparable with Bloch wall width [1].

•A Bloch and Néel walls can be approximated by an infinite elliptical cylinder, of height equal to the thickness of the film [1,2], placed between regions of opposite magnetization:

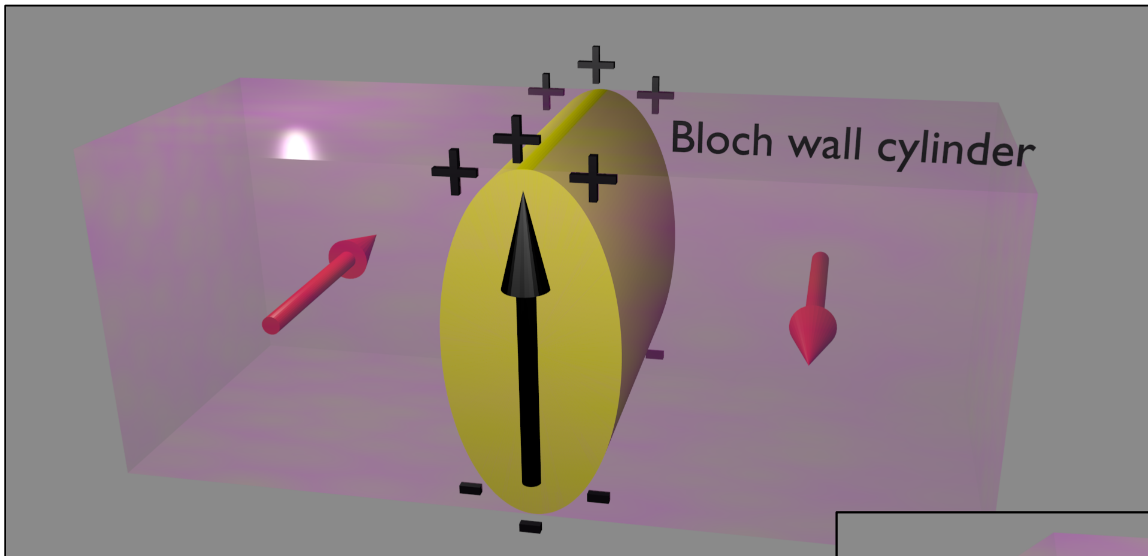

•Demagnetizing factors of the cylinders are approximated by expressions for ellipsoids.

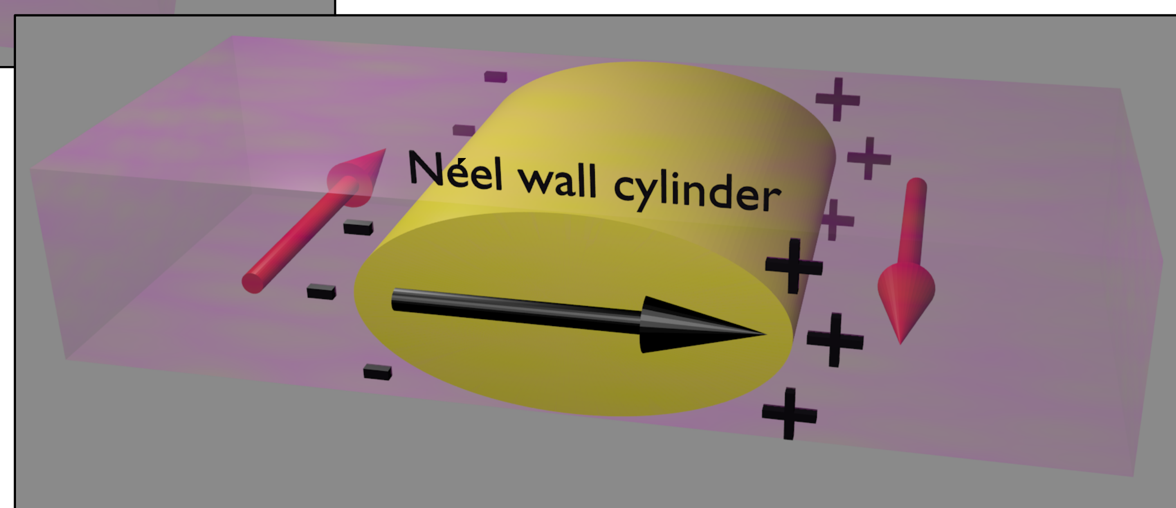

Domain walls in thin films

•Magnetic films are defined as **thin** if their thickness is comparable with Bloch wall width [1].

•A Bloch and Néel walls can be approximated by an infinite elliptical cylinder, of height equal to the thickness of the film [1,2], placed between regions of opposite magnetization.
•Within the cylinder demagnetizing field is created (N is taken from general expression**):

$$H_d = M_e N = \frac{M_e w}{w+t},$$

M_e - effective magnetization of the wall (see below)

t- film thickness
w -wall width

•Magnetostatic energy associated with that field is:

$$E_d = \frac{1}{2}\mu_0 N M_e^2 = \mu_0 \frac{M_e^2 w}{w+t} \qquad (1)$$

•The spin angle within the wall is supposed to change according to the expression*:

$$\phi = \pi(x/a) \quad for \quad -a/2 \le x \le a/2$$

a - wall width, φ – the angle between the magnetization and a direction in the plane of the wall and perpendicular to the plane of the film

•For a given φ(x) dependence the anisotropy energy density (averaged along the wall width) is:

$$E_A = \frac{1}{a}\int_{-a/2}^{a/2} K \cos^2[\pi(x/a)]\,dx = \frac{1}{2}K$$

*this is just an assumption, without proof; S. Middelhoek, J. Appl. Phys. 34, 1054 (1963)
** Eq. 3.23 in [1]; in numerator we have the shorter axis of the ellipsoidal cross section of the cylinder

Domain walls in thin films

- To find the effective magnetization of the Bloch wall in very thin films* ($t \ll w$) we calculate the magnetostatic energy of the wall in its own demagnetizing field:

$$E_d = \frac{\mu_0}{a} \int_{-a/2}^{a/2} 1 \cdot M_S^2 \cos^2 [\pi (\frac{x}{a})] dx = \frac{1}{2} \mu_0 M_S^2$$

demag factor for thin film

- Comparing this with Eq.(1) for $t \ll w$ we obtain:

$$E_d = \mu_0 \frac{M_e^2 w}{w+t} \approx \mu_0 M_e^2$$

$$M_e = \frac{M_s}{\sqrt{2}}$$

The Bloch wall can be approximated by the infinite cylinder if we decrease magnetization by a factor of 0.7... It is further assumed that this is true for thicker films too.

- The total energy of the wall (per unit area) is obtained by summing exchange, magnetocrystalline and stray field energy densities (volume energy densities are multiplied by wall thickness):

$$\gamma = A \left(\frac{\pi}{a} \right)^2 a + \frac{1}{2} K a + \mu_0 \frac{M_e^2 a}{a+t} a$$

$$\cos(x) = 1 - \frac{x^2}{2} + \ldots$$

- The energy is minimized with respect to wall width *a* and that value is inserted back in the expression for the energy.

*we can then use the approximation that the demag field at *x* depends only on magnetization at x.

S. Middelhoek, J. Appl. Phys. 34, 1054 (1963)

Domain walls in thin films

- The same kind of approximate calculations can be performed for Néel wall
- The wall is represented by the cylinder as in the case of Bloch wall, but it is now flattend; as a consequence the demagetization coefficient changes:

$$H_d = M_e N = \frac{M_e t}{w+t}, \qquad M_e$$ - effective magnetization of the wall (see below)

- It is assumed that the effective magnetization is the same as in the case of “Bloch cylinder”.
- For Néel wall the expression for the total energy is then:

$$\gamma = A\left(\frac{\pi}{a}\right)^2 a + \frac{1}{2} K a + \mu_0 \frac{M_e^2 t}{a+t} a$$

the only difference between Néel and Bloch walls within the present model

- The energy and domain wall width dependence on film thickness can be obtained numerically. Here the exemplary *Mathematica* code:

```
A=1;
mi0=1;
K=1;
Ms=1;
energyNeel[a_,t_]=A (Pi^2/a)+0.5 a K+(0.5 mi0 Ms^2 a t/(a+t));
tmax=40;
ilepunktow=201;
w=Table[{t//N,FindMinimum[energyNeel[x,t],{x,2}][[2,1,2]]},{t,0,tmax,tmax/(ilepunktow-1)}];
ListPlot[w,Joined->False] (*wall width versus film thickness*)
energiavsthickness=Table[{i tmax/(ilepunktow-1)//N,energyNeel[w[[i,2]],i tmax/(ilepunktow-1)]},{i,1,ilepunktow,1}];
ListPlot[energiavsthickness,Joined->False](*wall energy versus film thickness*)
```

S. Middelhoek, J. Appl. Phys. 34, 1054 (1963)

Energy of Bloch and Néel wall

•In case of thin films the most important difference between those kinds of domain walls is their dependence on film thickness:

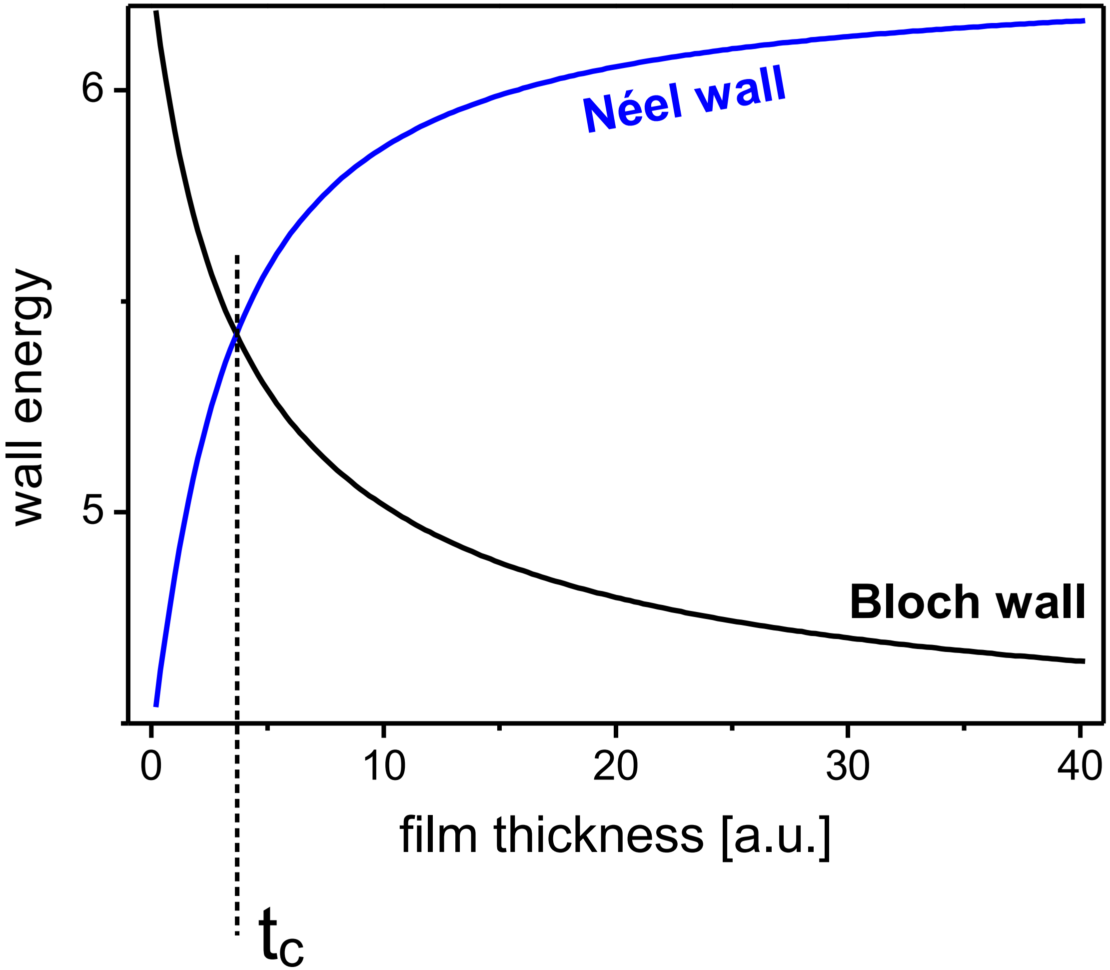

• At certain critical thickness the energy of Néel wall becomes less than the energy of Bloch wall

•The Néel walls are favored in thin easy-plane anisotropy films

•In thin perpendicular anisotropy films Bloch walls may be energetically favored

S. Middelhoek, J. Appl. Phys. 34, 1054 (1963)

Energy of Bloch and Néel wall

•The same model predicts the thickness dependence of domain wall width:

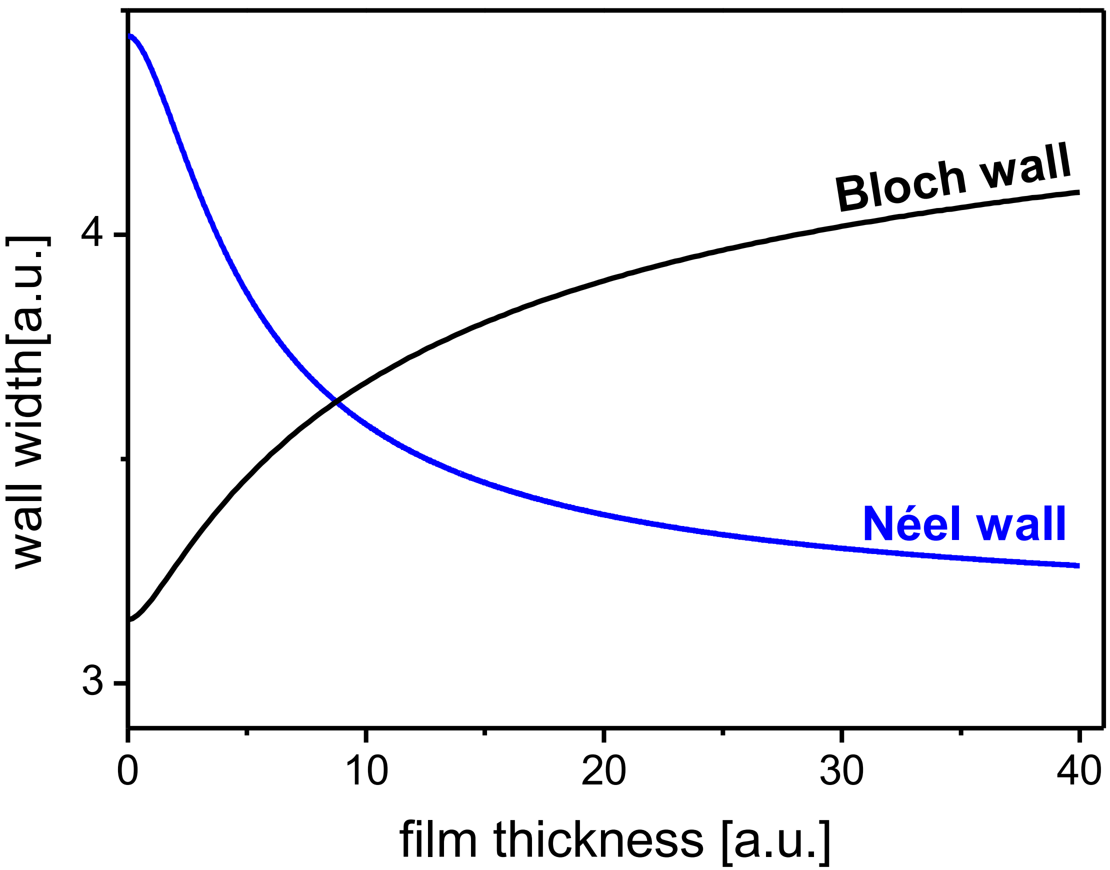

•Néel walls are characterized by core region with dipolar charge pattern (see 12 pages back) and long tails

•The more elaborate calculations give that core width can be expressed as:

$$W_{core}=2\sqrt{\frac{A}{(K_u+K_d)(1-c_o^2)}}$$

c_0 is a cosine of the spin angle corresponding to core-tail boundary.

•The spin angle of Néel wall is, similarly to Bloch wall, field dependent

•With increasing K_d core width decreases and tails get longer

•In permalloy $\sqrt{A/K_d}$ is about 5 nm [1]

Energy of Bloch and Néel wall

•The critical thickness of the Bloch-Néel wall transition is of the order of tens of nanometers:

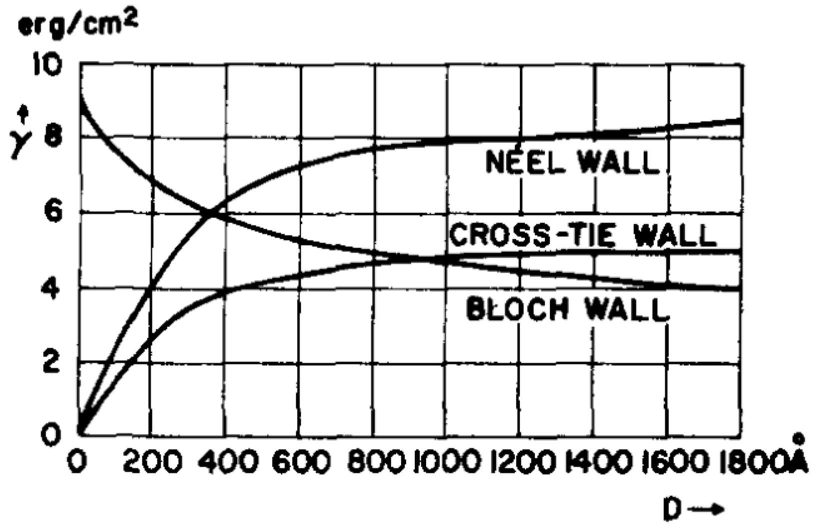

FIG. 1. Energy per unit area of a Bloch wall, a Néel wall and a cross-tie wall as a function of the film thickness [$A=10^{-6}$ ergs/cm, $M_S=800$ G, and $K=1000$ ergs/cm^3].

•Other types of walls exist which can have lower energy then Bloch or Néel walls depending on thickness, external field value etc.:

-cross-tie walls

-asymmetric Bloch and Néel walls

S. Middelhoek, J. Appl. Phys. 34, 1054 (1963)

Cross-tie walls

- At intermediate thicknesses cross-tie walls exists
- They are composed of alternating regions of Bloch and Néel-like transitions
- In permalloy films they are observed for thickness range from 30 to 90 nm
- Shematic view of cross-tie wall:

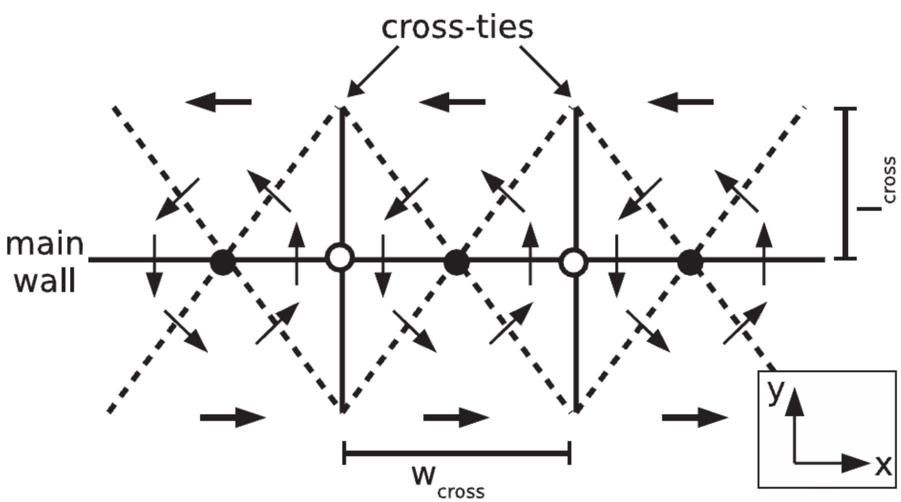

Fig. 1: Schematic of a cross-tie domain wall.

N. Wiese et al., EPL 80, 57003 (2007)

- Note the change of the cross-ties spacing as a function of the effective anisotropy (introduce by bending of the film – stress anisotropy)

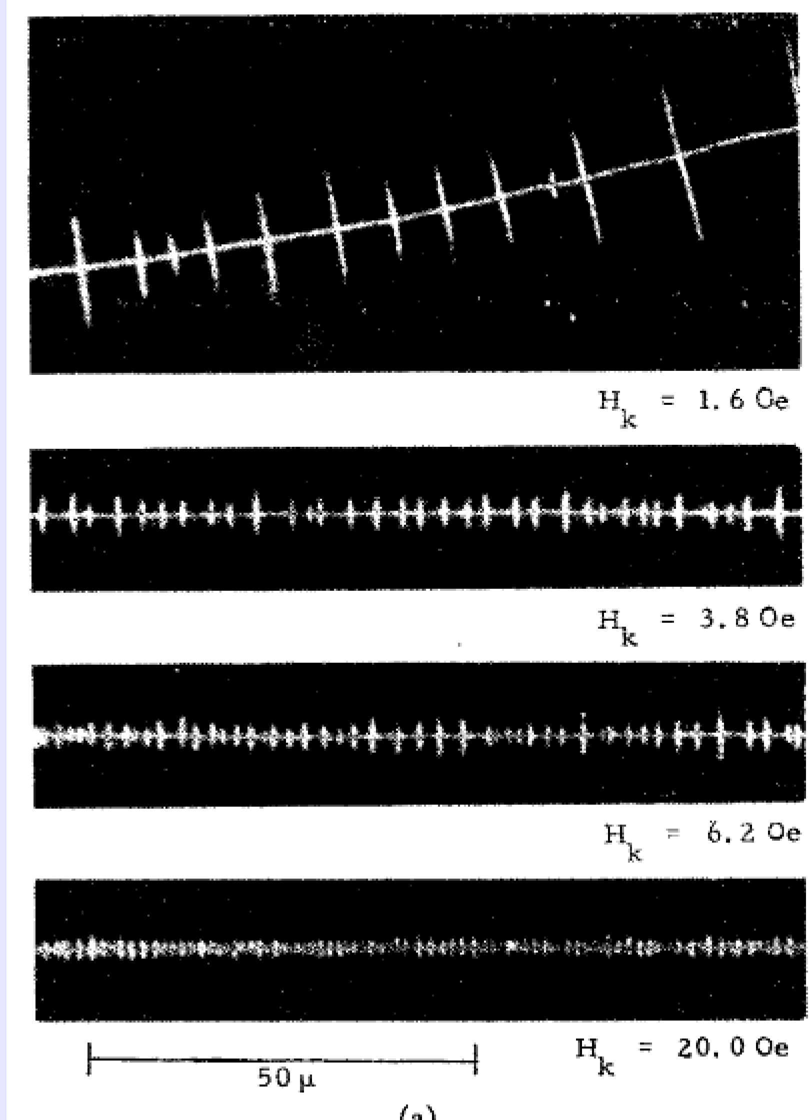

Bitter patterns of a cross-tie wall for different anisotropy fields H_K

S. Middelhoek, J. Appl. Phys. 34, 1054 (1963)

Cross-tie walls

- The inner structure of the cross-tie walls can be resolved with contemporary imaging methods.

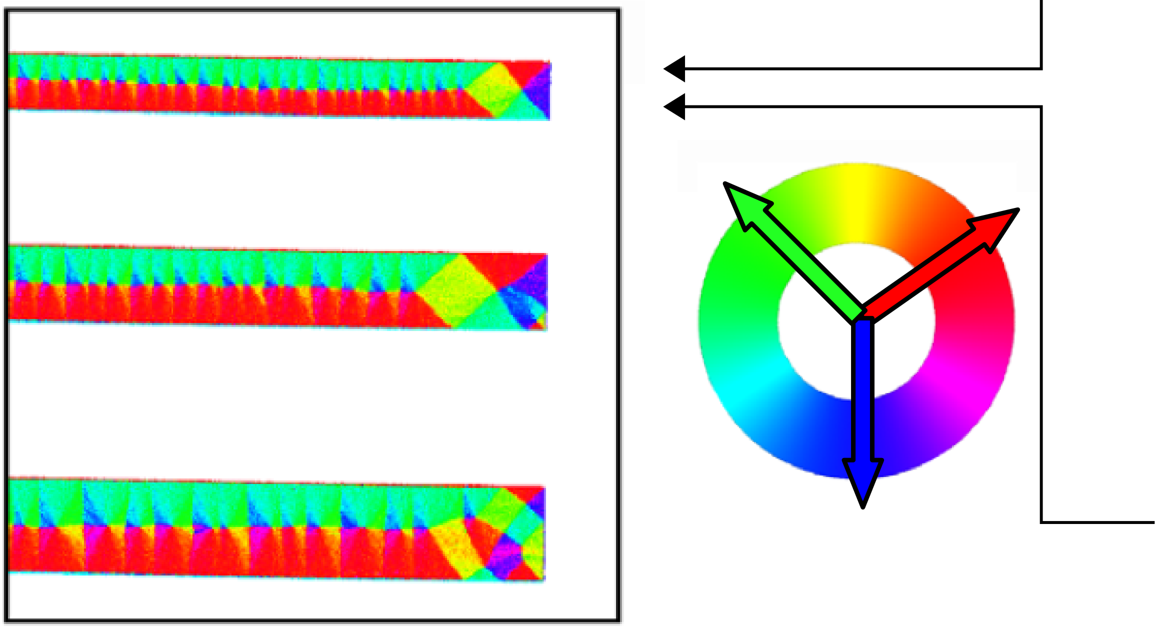

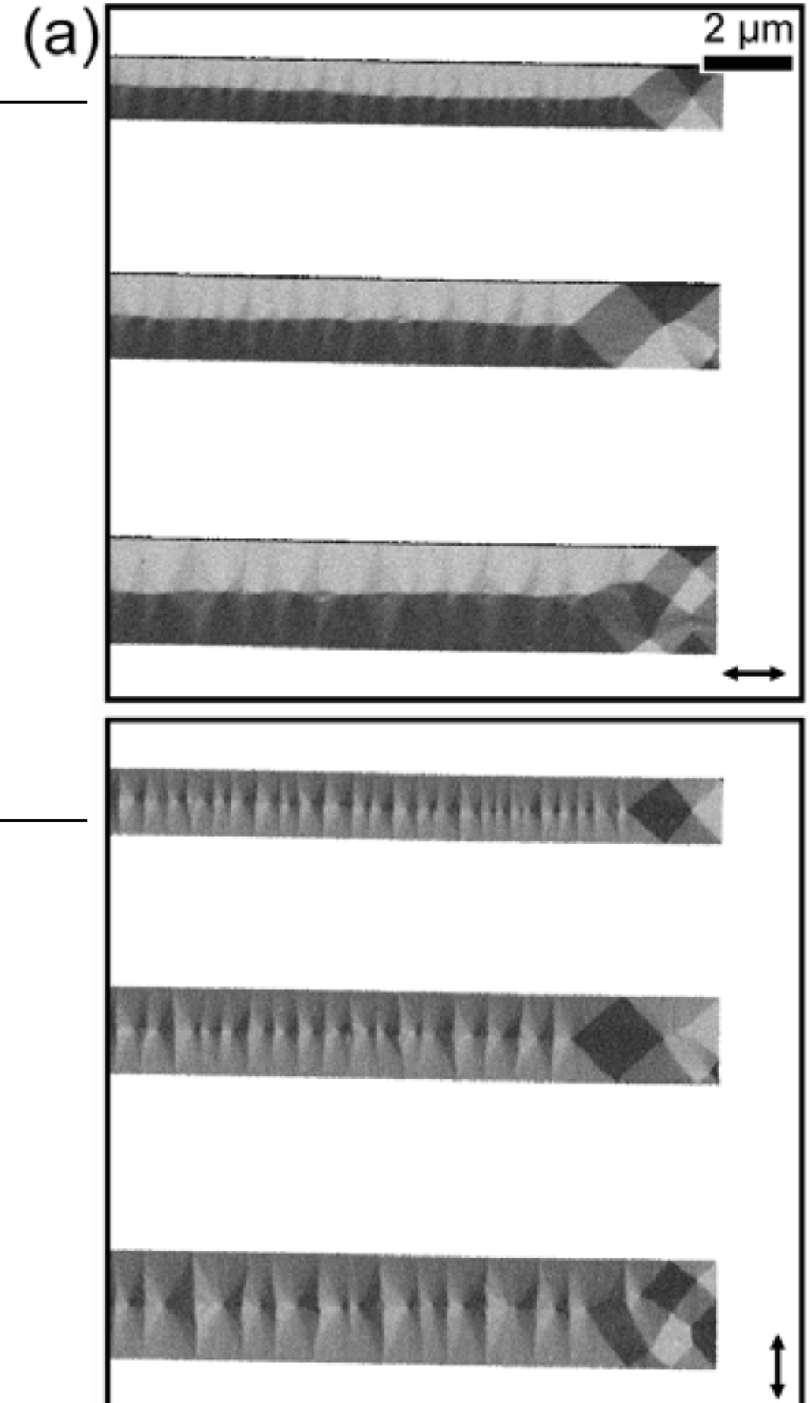

Fig. 2: (Colour on-line) DPC images of elements with constant aspect ratio, $\ell/w = 10$, and varying width of (a) $1.5 < w < 2.5\,\mu$m, (b) $w = 1.25\,\mu$m, and (c) $w = 0.5\,\mu$m. The direction of sensitivity has been chosen parallel and perpendicular to the long axis of the elements, respectively, as indicated by the arrows. The third image in each set shows the angular distribution of the induction within the elements, calculated from the two vector components.

N. Wiese et al., EPL 80, 57003 (2007)

Cross-tie walls

•The cross-tie wall images obtained from Lorentz microscopy* confirm the predicted structure of the transition region:

R. Ploessl et al., J. Appl. Phys. 73, 2447 (1993)

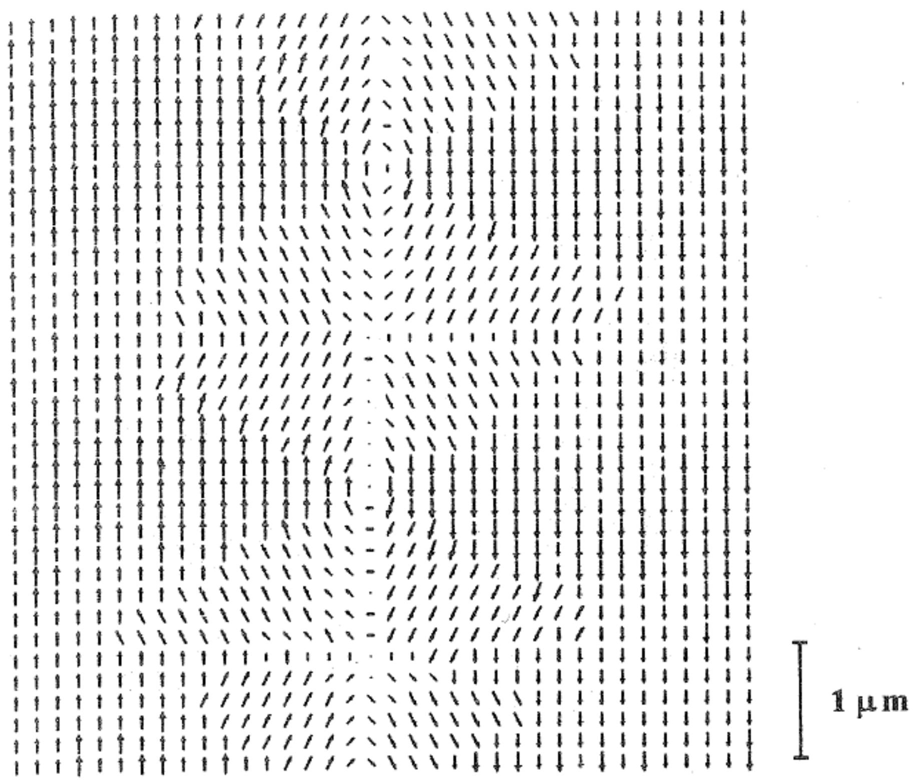

FIG. 4. Corresponding vector map to Fig. 3.

Cross-tie structure of the evaporated 60 nm thick permalloy film (*from Lorentz electron microscopy image*).

*detects the force acting on imaging electrons due to magnetic field

Asymmetric walls

•In some cases asymmetry of the spin angle in domain wall may result in **stray-field free** domain walls in thin films:

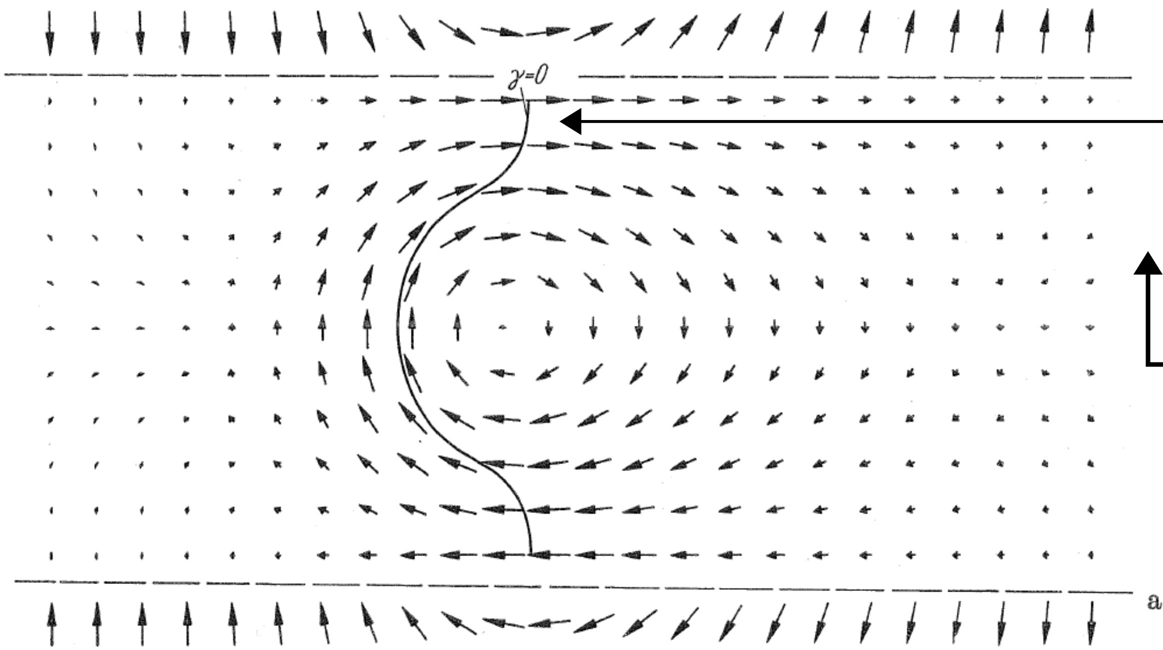

4. Vector diagrams of asymmetric Bloch walls. These models are more or less valid for all film thicknesses.
a) $h = 0$

The contour line indicates the "center" of the wall, i.e. the surface on which z-component of magnetization passes through zero

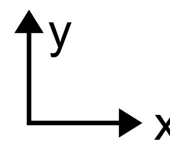

A. Hubert, phys.stat.sol. 38 699(1970)

•In "normal" walls "center" of the wall is planar

•Similarly stray-field free configurations can be obtained for Néel walls [1].

Asymmetric walls

- Depending on film thickness and external field value various kinds of domain wall are energetically favored:

A. Hubert, phys.stat.sol. 38 699(1970)

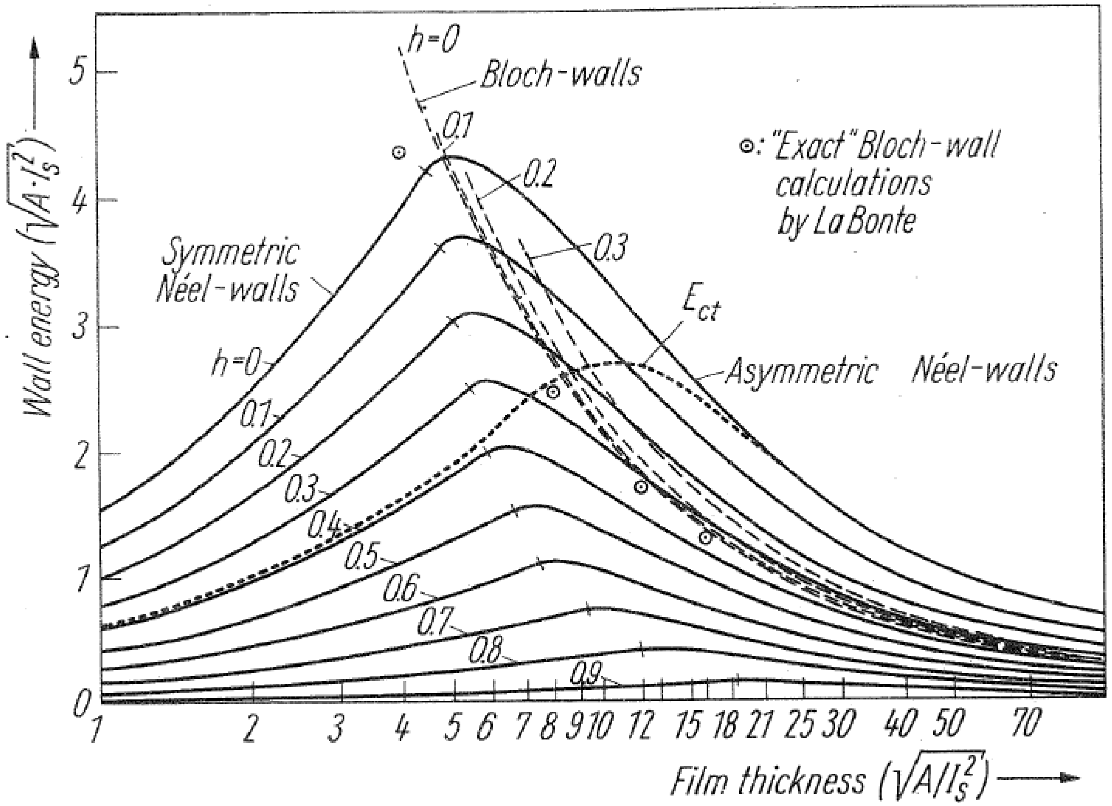

Fig. 1. The total wall energies per unit wall surface as a function of film thickness. Parameter is the reduced applied field $h = H\, I_s/(2\, K)$. $K/I_s^2 = 1/640$

$$h = H \frac{\mu_0 M_S}{2K}$$

- Bloch walls are only stable compared to Néel walls up to reduced field h=0.3.

360° walls

- In thin films two Néel walls of the opposite rotation sense (unwinding walls) attract each other each other – because they generate opposite charges in their overlaping tails [1].
- In thin films two Néel walls of the same rotation sense (winding walls) repel each other:

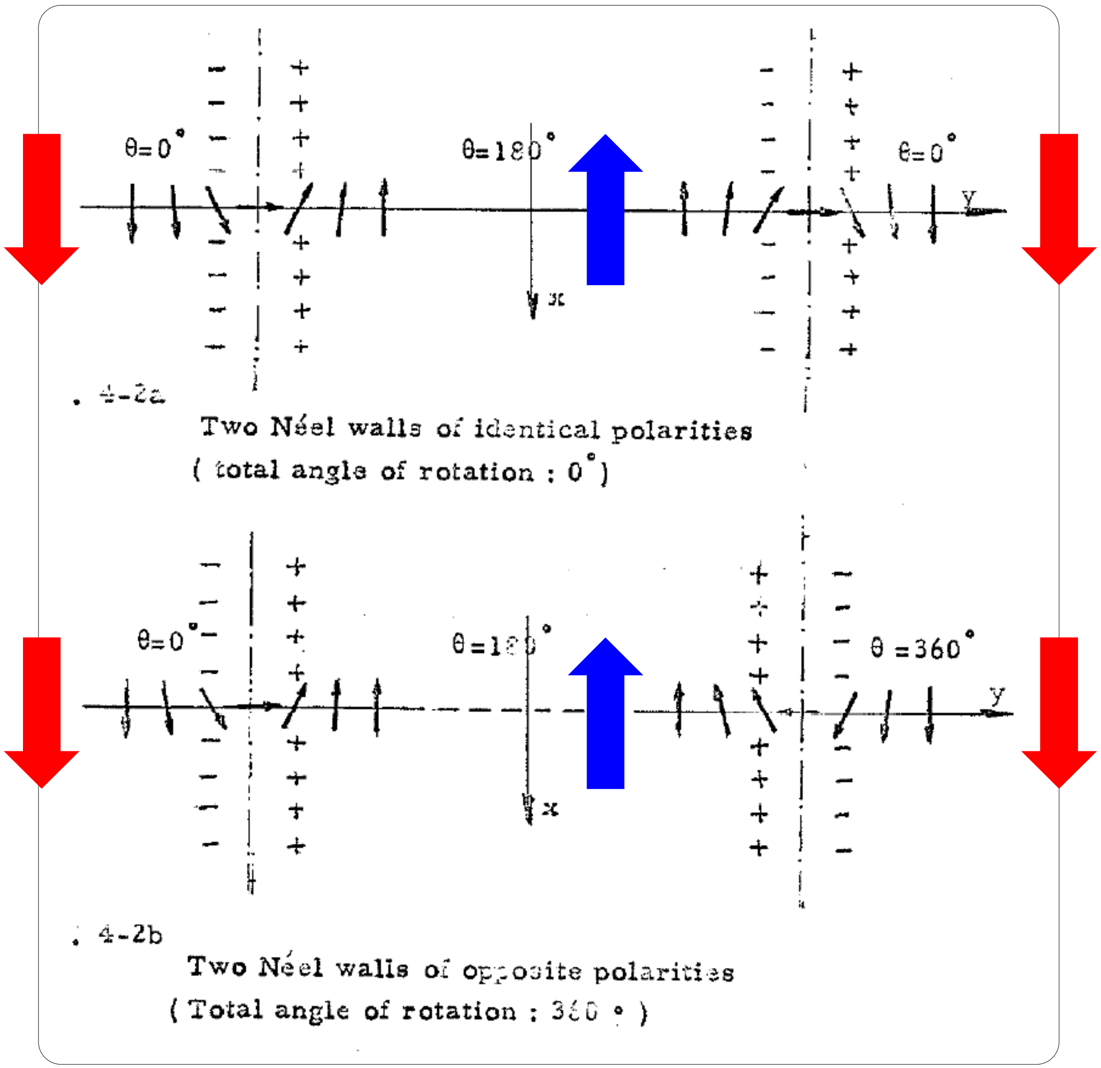

- When to unwinding walls meet they can annihilate
- If the winding walls are pressed together by the action of the external field energetically disfavoring the magnetization direction within the walls (blue arrow) they create so called 360° wall.
- The 360° wall can be annihilated only in large fields [1].
- In permalloy films of 50nm thickness Néel walls interact over distances at least **0.1mm!** (2000 times the thickness)

R.C. Collette 1964, dissertation, Pasadena 1964

360° walls

•From the point of view of applications 360° walls should be avoided as they may reduce the reproducibilty of switching events*

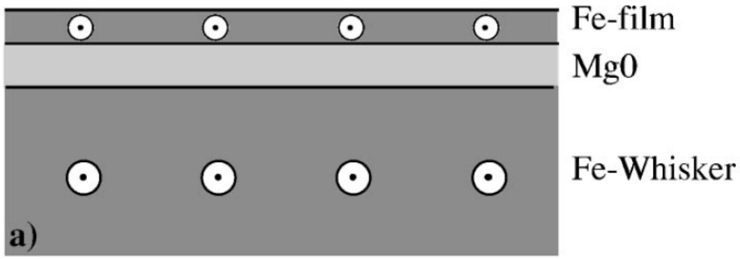

The domain structure in Fe layer and whisker is the same due to magnetostatic interactions

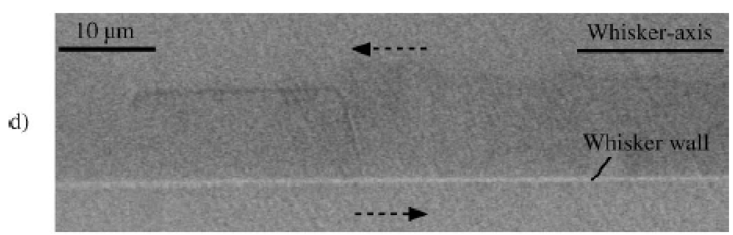

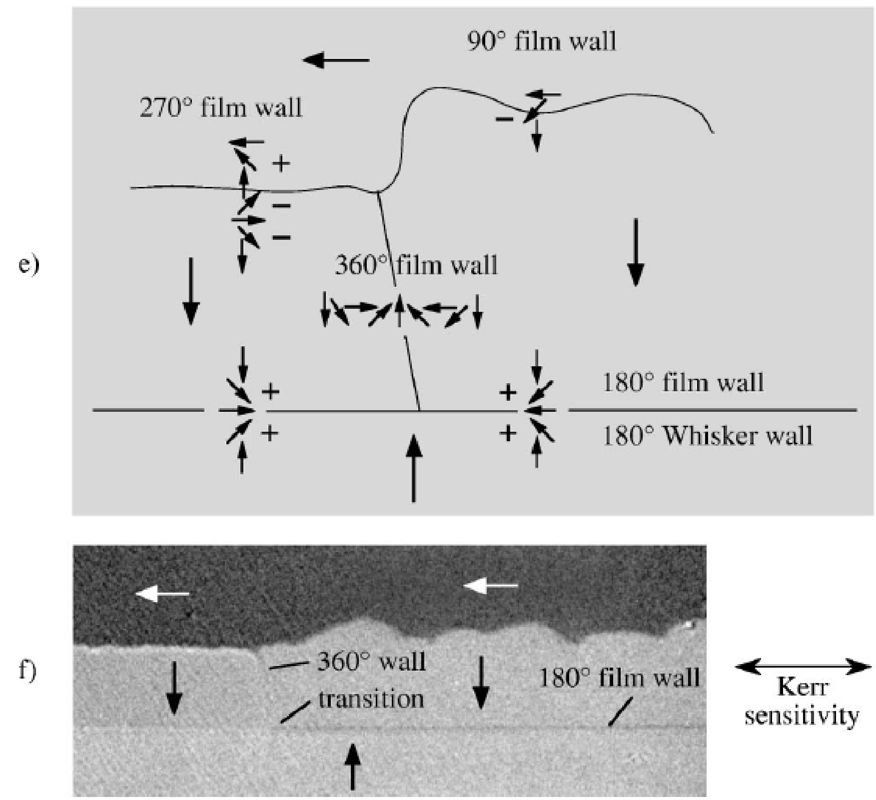

FIG. 5. (a) Domain pattern in the iron film, containing 360° domain walls. The formation of 360° walls is shown by film-selective images in (b) and (c). The domain state of (c) is selectively imaged in (d) by whisker. Wall segments of certain polarities are responsible for the formation of 360° walls as explained schematically in (e). The expected change in chirality of the 180° film wall is verified in (f).

R. Schäfer et al., PHYSICAL REVIEW B **65**, 144405 (2002)

*C. B. Muratov and V. V. Osipov J.Appl. Phys. **104**, 053908 (2008)

360° walls

•Domain walls can be generated by the proper external field sequence:

other sample- two 180° walls

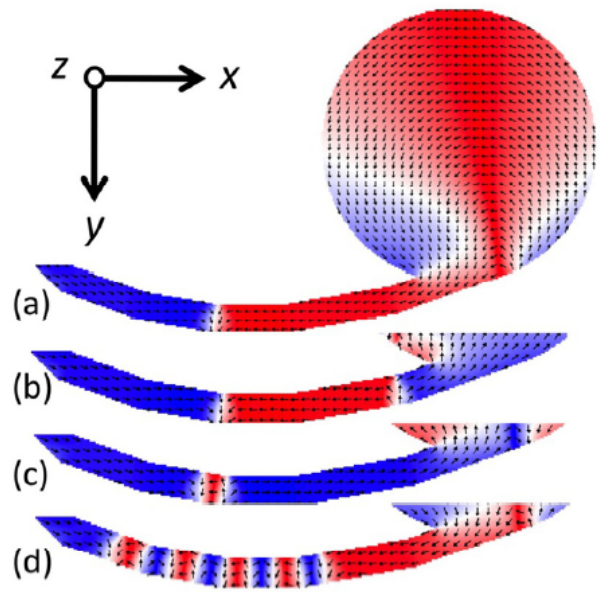

FIG. 1. (Color online) OOMMF model of formation of 360DW in a wire attached to a circular pad. (a) After 239 kA/m saturation along y, a 180DW formed in the wire, shown at remanence. (b) A further field of -4.0 kA/m along y produced a second 180DW. (c) The remanent state showing a 360DW. (d) Repeated alternating field of magnitude 9.5 kA/m along y generated multiple domain walls. Red and blue (or greyscale shading) represent the sign of the x-component of the magnetization.

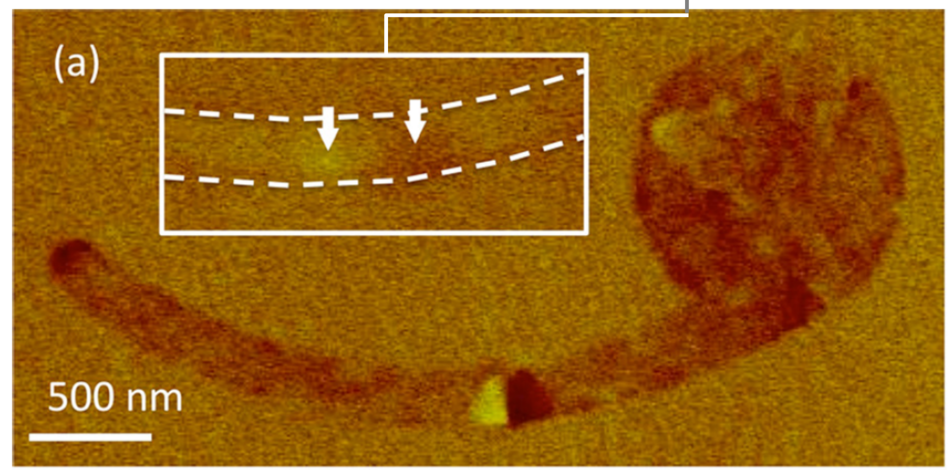

imaged at a tip height of **20 nm**

5nm thick Co structure
4×4×5 nm³ micromagnetic cells

Field sequence:
- 239 kA/m saturation along y- direction
- remanence - 180° wall generated
- -15.9 kA/m field produced the second 180° wall
- remanence – two 180° walls meet to create 360° wall

•Results of micromagnetic simulations are confirmed by Magnetic Force Microscopy images

Youngman Jang etal., APPLIED PHYSICS LETTERS 100, 062407 (2012)

540^{o} walls

•Inserting a consequtive 180^{o} wall to the wire with 360^{o} wall can create 540^{o} wall:

Appl. Phys. Lett. **100**, 062407 (2012)

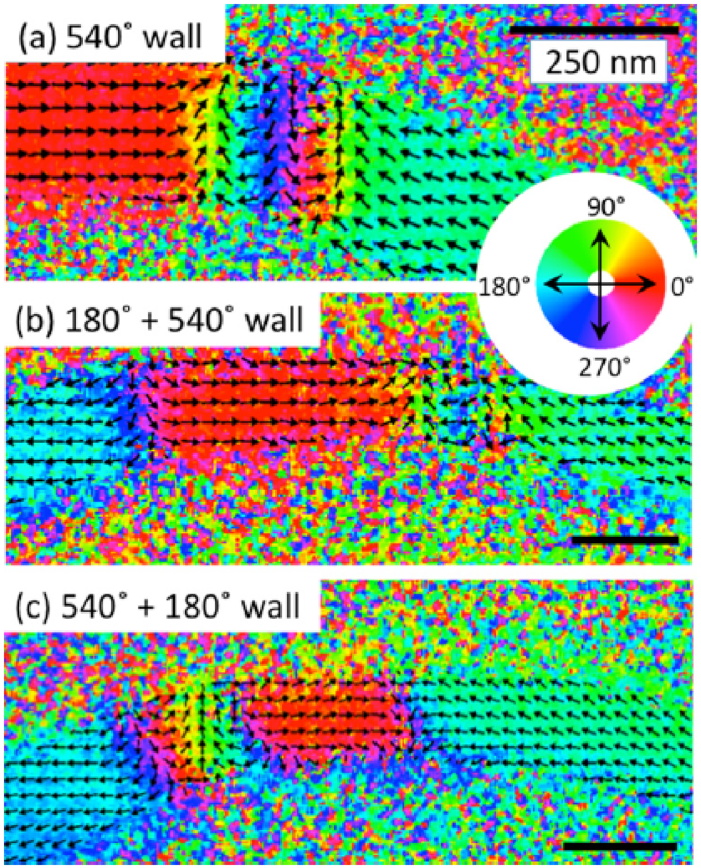

FIG. 4. (Color online) (a) SEMPA image of a 540DW. (b) SEMPA image after injecting an additional 180DW. (c) A 540DW of opposite sense to that of (a) adjacent to a 180DW. Magnetization directions are indicated on a color wheel. The uncertainty in the SEMPA angular data is 7.4° (one standard deviation). Scale bars are 250 nm.

SEMPA* images suggest the possibility of producing higher order walls – wit nπ rotation

•360^{o} walls have well-defined structure and persist over wide field range

Youngman Jang etal., APPLIED PHYSICS LETTERS 100, 062407 (2012)

*SEMPA-scanning electron microscopy with polarization analysis

Magnetic whiskers

- Due to almost **perfect crystallinity** whiskers are ideal for the investiagtions of simple domain structures [1].
- Whiskers are usually grown from vapour phase by chemical reactions
- Process parameters (temperature, pressure etc.) control the sizes, type and the perfection of the whiskers
- The whiskers can be up to several milimiters in size
- Domain observation is possible from all sides [1].
- Typical domain structure of whisker:

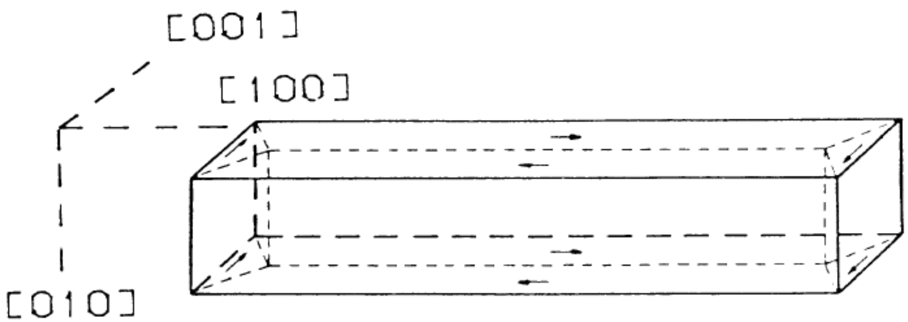

FIG. 1. Landau domain structure of an iron whisker grown in a ⟨100⟩ crystallographic direction and bounded by {100} faces.

J. Phys. D: Appl. Phys. **45** (2012) 085001

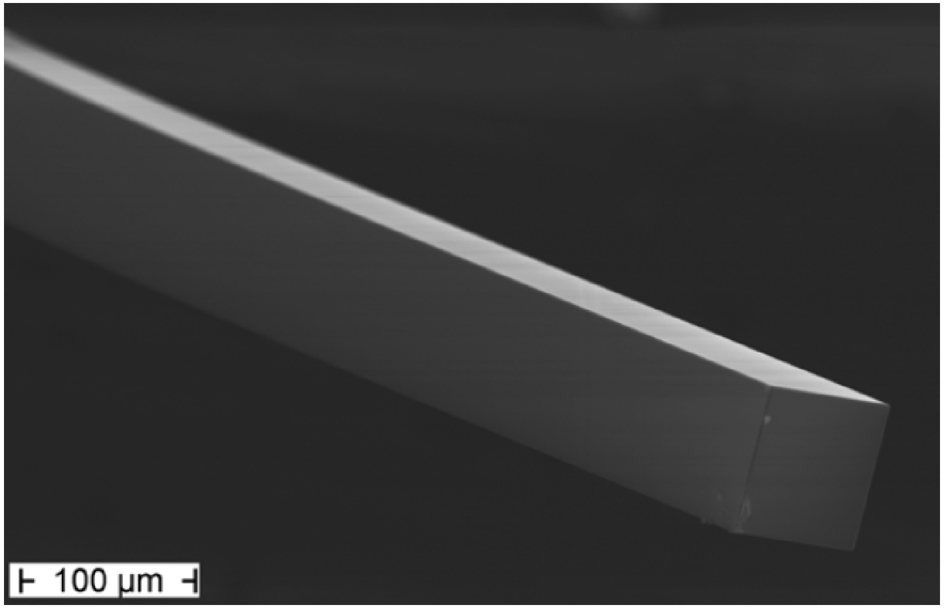

M. Langosch, H. Gao, U. Hartmann

Figure 1. SEM image of an iron whisker with ⟨1 0 0⟩ growth direction.

U. Hartmann, Phys. Rev. B **36**, 2331 (1987)

Magnetic whiskers

•Due to almost **perfect crystallinity** whiskers are ideal for the investiagtions of simple domain structures [1].

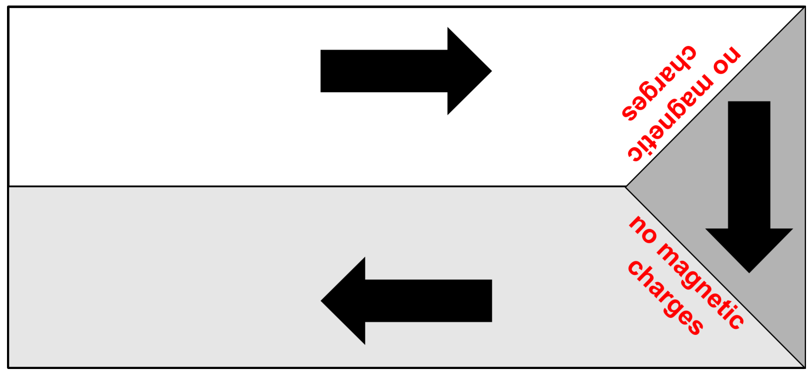

perfect **closure domains** produce no magnetic fields

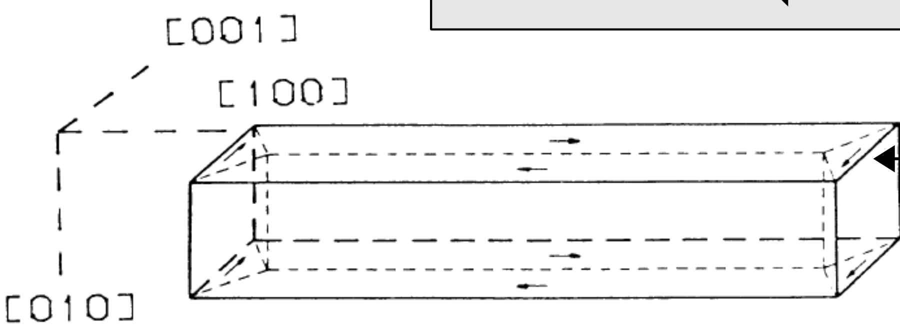

FIG. 1. Landau domain structure of an iron whisker grown in a ⟨100⟩ crystallographic direction and bounded by {100} faces.

U. Hartmann, Phys. Rev. B **36**, 2331 (1987)

Magnetic whiskers

- **Brown's coercive paradox** – coercive fields predicted by the early (1940s) calculations hugely overestimated the experimental results.
- Brown predicted, assuming ellipsoidal shape of the sample, that the reversal (coercive) field should be:

$$H_r > \frac{2K}{\mu_0 M_s} - N_d M_s$$

- In whiskers "*huge demagnetizing fields associated with a uniformly magnetized corner cause the formation of closure domains (...) which remain even during the overall magnetization of the whisker.*" (U. Hartmann).

- The whisker electropolished in CrO_3 glacial acetic acid show greatly increased coercive field and hysteresis characteristic for single-domain particles.

Polished whiskers have much higher coercive fields

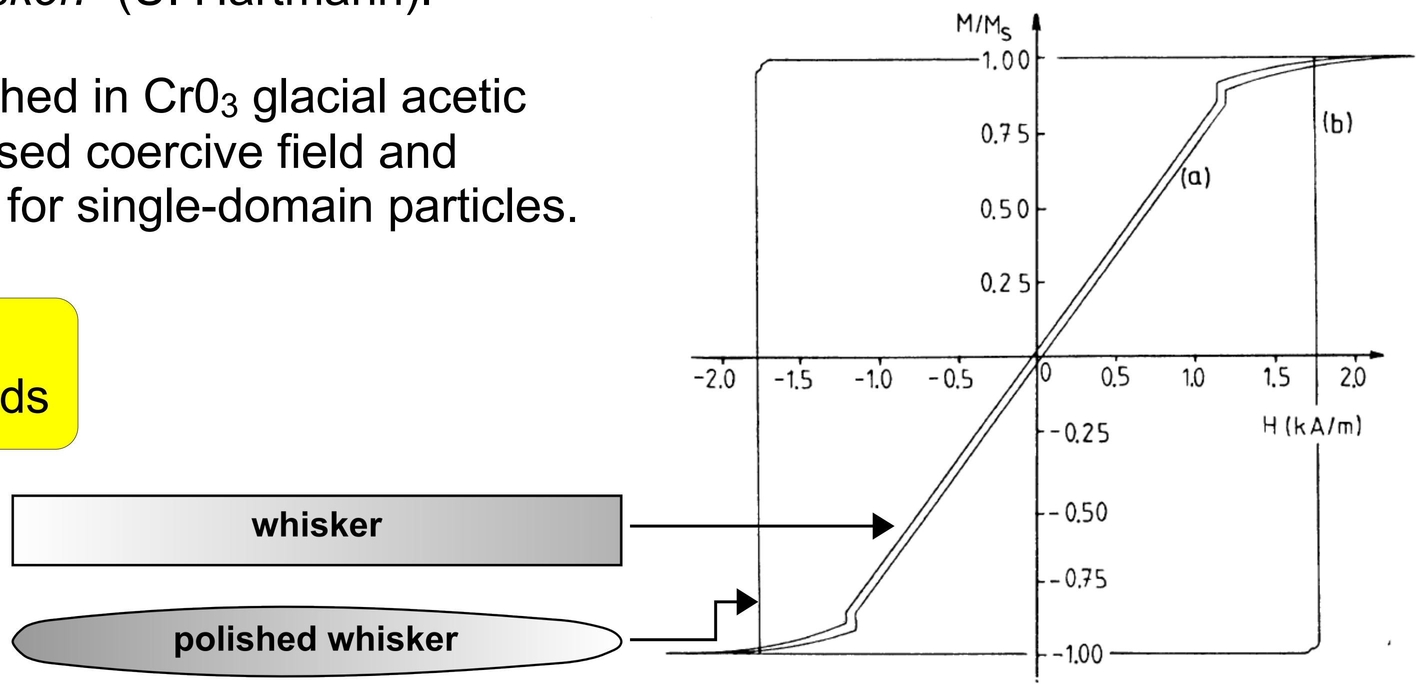

FIG. 2. (a) Magnetization curve of a whisker in the as-grown state, (b) after smoothing of the whisker tips.

U. Hartmann, Phys. Rev. B **36**, 2331 (1987)

Magnetic wires

- In contrast to whiskers they do not have, in general, perfect structure
- Amorphous magnetic wires find applications in sensors
- Due to the high curvature of the surface modifications of standard domain imaging methods must be employed. On of the methods is the magneto-optical indicator film (MOIF) microscopy:

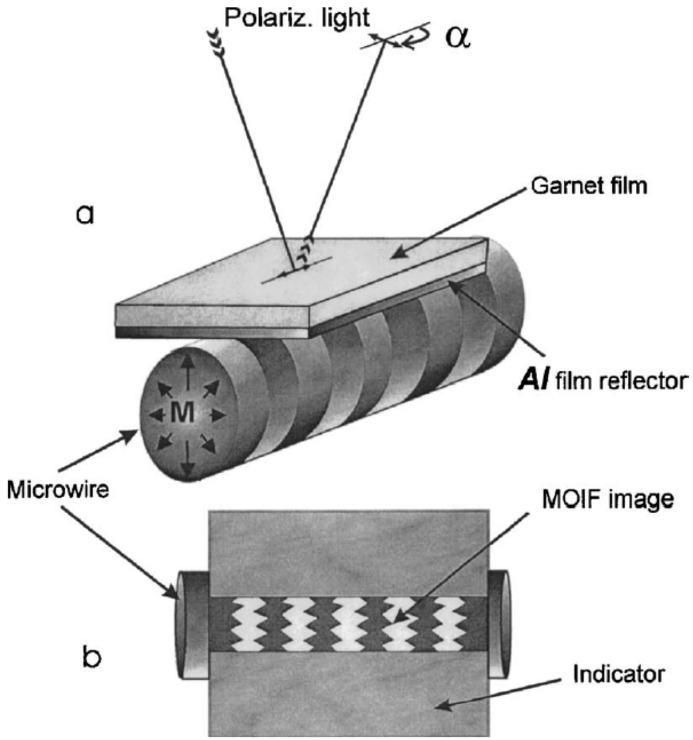

FIG. 1. Schematic picture showing the experimental setup configuration (a) and the MOIF images from Fe-rich wire (b).

- Magnetic moments within garnet indicator film with high Verdet constant are influenced by the stray fields coming from the surface of the wire
- The changes in magnetic structure of the indicator film are detected by the Faraday effect which is sensitive to the magnetization component parallel to incident light.

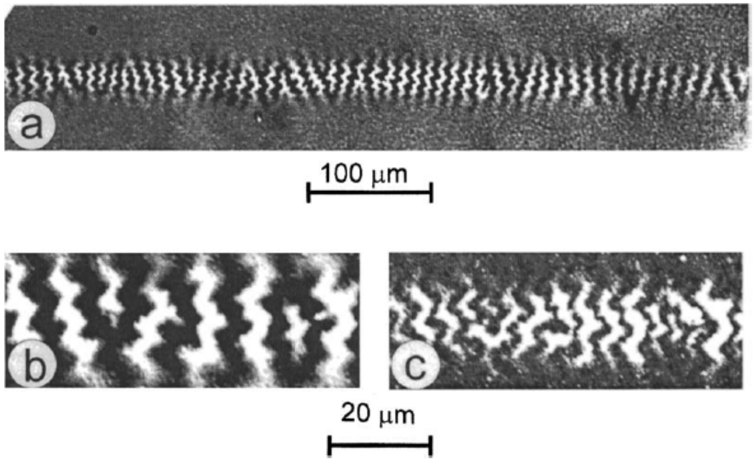

FIG. 2. Magneto-optical contrast of the magnetization distribution on the surface of the Fe-rich wire (a, b) and (c) MOIF image of the domain walls in the region as indicated in (b).

Yu. Kabanov, A. Zhukov, V. Zhukova, and J. Gonzalez, APPLIED PHYSICS LETTERS 87, 142507 (2005)

Magnetic wires

- In contrast to whiskers they do not have, in general, perfect structure
- Amorphous magnetic wires find applications in sensors
- Due to the high curvature of the surface modifications of standard domain imaging methods must be employed. On of the methods is themagneto-optical indicator film (MOIF) microscopy.

- Labirynth-like *open domain structure** is present in the wire

- In Fe-rich wires ($Fe_{77.5}B_{15}Si_{7.5}$), with **positive magnetostrictions, the magnetic moments are perpendicular to the surface** in the regions close to surface and the domains are separated by 180^o walls.

- In Co-rich wires ($Co_{72.5}B_{15}Si_{12(?)}$), with negative magnetostriction, magnetic moments are parallel to the surface of the wire

- The core of the wire is magnetized approximately along the wire axis with domains no less than 0.5mm in size.

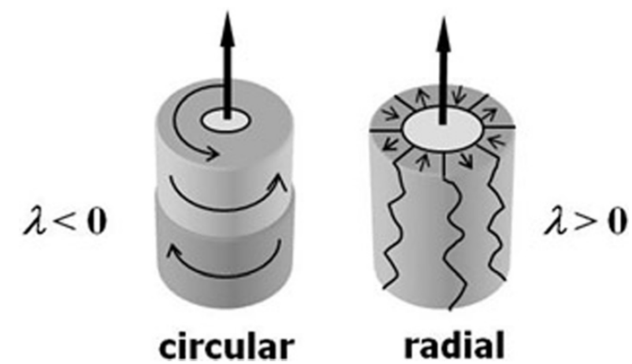

FIG. 1. Domains with circular and radial magnetization.

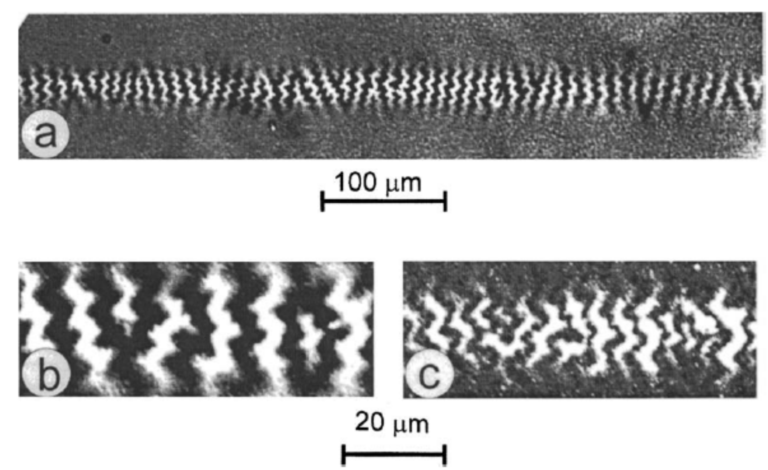

FIG. 2. Magneto-optical contrast of the magnetization distribution on the surface of the Fe-rich wire (a, b) and (c) MOIF image of the domain walls in the region as indicated in (b).

image from: N. N. Orlova, A. S. Aronin, S. I. Bozhko, Yu. P. Kabanov, and V. S. Gornakov, J. Appl. Phys. 111, 073906 (2012)

*that is without closure domains

Yu. Kabanov, A. Zhukov, V. Zhukova, and J. Gonzalez, APPLIED PHYSICS LETTERS 87, 142507 (2005)

Landau-Lifshitz-Gilbert (LLG) equation of spin motion

- The change of angular momentum of a rigid body under the influence of the torque is given by:

$$\vec{\tau} = \frac{d\vec{J}}{dt}$$

- The torque acting on magnetic moment in magnetic field is: $\vec{\tau} = \vec{m} \times \vec{B}$
- With gyromagnetic ratio (L.1) defined as $\gamma = \frac{|\vec{m}|}{|\vec{J}|}$ we get:

For an electron we have:

$$\vec{m}_e = -g_e \frac{e}{2m} \vec{S}$$

$$\boxed{\frac{d\vec{m}}{dt} = \gamma \vec{m} \times \vec{B}}$$

This equation can be used to describe motion of the electron's magnetic moment. The electron itself is fixed in space.

- Larmor precession [3]

Vector rotating with angular velocity Ω changes according to the formula:

$$\frac{d\vec{A}}{dt} = \vec{\Omega} \times \vec{A}$$

- Consider a rotating coordinate system in which vector A is not constant. Then the rate of change of that vector in inertial (resting, laboratory) coordinate system is given by:

$$\left(\frac{d\vec{A}}{dt}\right)_{inert} = \left(\frac{d\vec{A}}{dt}\right)_{rot} + \vec{\Omega} \times \vec{A}$$

Landau-Lifshitz-Gilbert (LLG) equation of spin motion

•Combining the previous equation with the expression for the rate of change of magnetic moment vector we obtain:

$$\frac{d\vec{m}}{dt} = \gamma\, \vec{m}\times\vec{B}, \quad \left(\frac{d\vec{A}}{dt}\right)_{inert} = \left(\frac{d\vec{A}}{dt}\right)_{rot} + \vec{\Omega}\times\vec{A}$$

$$\left(\frac{d\vec{m}}{dt}\right)_{rot} = \left(\frac{d\vec{m}}{dt}\right)_{inert} - \vec{\Omega}\times\vec{A} = \gamma\, \vec{m}\times\vec{B} - \vec{\Omega}\times\vec{m}$$

$$\left(\frac{d\vec{m}}{dt}\right)_{rot} = \gamma\, \vec{m}\times\vec{B} + \vec{m}\times\vec{\Omega} = \gamma\, \vec{m}\times\left(\vec{B} + \frac{\vec{\Omega}}{\gamma}\right)$$

•If $\vec{B} + \frac{\vec{\Omega}}{\gamma} = 0$ then the magnetic moment ***m*** is constant in rotating frame. It means that it rotates with angular velocity Ω relative to inertial frame.

•The velocity is called *Larmor angular velocity* and is given by:

$$\boxed{\vec{\Omega}_L = \gamma\, \vec{B}}$$

•The corresponding *Larmor frequency* is:

$$f_L = \frac{1}{2\pi}\gamma\, B$$

•For electron *Larmor frequency* is approximately 1.761×10^{11} rad $s^{-1}T^{-1}$ *

*http://physics.nist.gov/cgi-bin/cuu/Value?gammae retrieved 2012.05.16

Landau-Lifshitz-Gilbert (LLG) equation of spin motion

•Landau and Lifshitz have introduced **a damping term** to the precession equation:

$$\frac{d\vec{m}}{dt}=\gamma\,\vec{m}\times\vec{B}-\frac{\alpha_L}{|\vec{m}|}\left(\vec{m}\times\left(\vec{m}\times\vec{B}\right)\right), \qquad (1)$$

where α_L is a dimensionless parameter [5].

•As can be seen the damping vector $-\vec{m}\times(\vec{m}\times\vec{B})$ is directed toward ***B*** and vanishes when ***m*** and ***B*** become parallel.

•As can be seen from Eq. (1) the acceleration of ***m*** towards ***B*** is greater the higher the damping constant α_L. Gilbert [6] pointed out that this is nonphysical and that Eq. (1) can be used for small damping only [5].

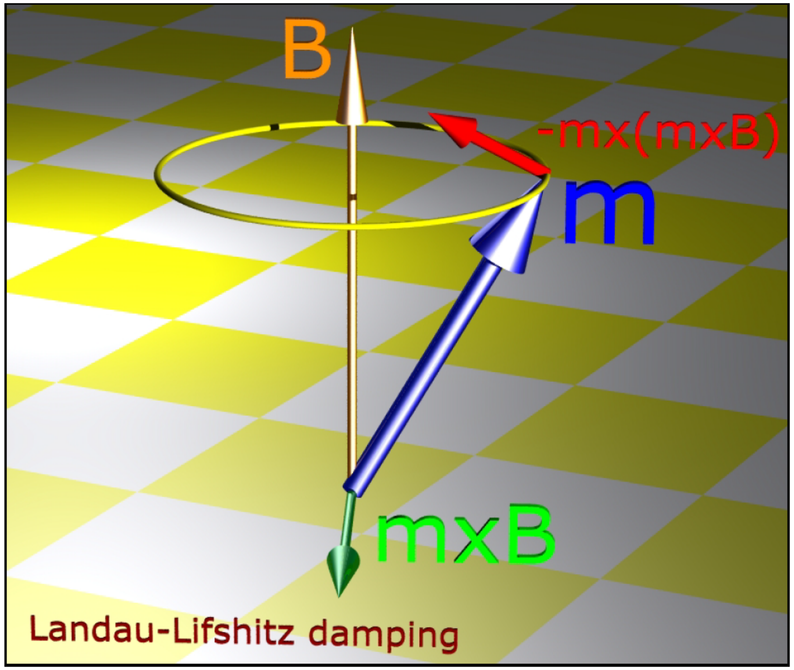

•He introduced other phenomenological form of equation which can be used for arbitrary damping. Damping is introduced as dissipative term [7] of the effective field acting on the moment:

$$\vec{B}\rightarrow\vec{B}-\eta\frac{d\vec{m}}{dt} \qquad (2)$$

Landau-Lifshitz-Gilbert (LLG) equation of spin motion

•Inserting Eq. (2) into precession eguation (3 slides back) we obtain:

$$\frac{d\vec{m}}{dt}=\gamma\,\vec{m}\times\vec{B}=\gamma\,\vec{m}\times\left(\vec{B}-\eta\frac{d\vec{m}}{dt}\right)=\gamma\,\vec{m}\times\vec{B}=\gamma\,\vec{m}\times\vec{B}-\gamma\,\eta\,\vec{m}\times\frac{d\vec{m}}{dt}=$$

$$\gamma\,\vec{m}\times\vec{B}-\frac{\alpha}{|\vec{m}|}\vec{m}\times\frac{d\vec{m}}{dt},\quad \text{with}\quad \alpha=\gamma\,\eta\,|\vec{m}|$$

$$\frac{d\vec{m}}{dt}=\gamma\,\vec{m}\times\vec{B}$$

$$\vec{B}\rightarrow\vec{B}-\eta\frac{d\vec{m}}{dt}$$

•The equation can be transformed by substituting itself into righ-hand side:

$$\frac{d\vec{m}}{dt}=\gamma\,\vec{m}\times\vec{B}-\frac{\alpha}{|\vec{m}|}\vec{m}\times\frac{d\vec{m}}{dt}=\gamma\,\vec{m}\times\vec{B}-\frac{\alpha}{|\vec{m}|}\vec{m}\times\left(\gamma\,\vec{m}\times\vec{B}-\frac{\alpha}{|\vec{m}|}\vec{m}\times\frac{d\vec{m}}{dt}\right)$$

•Multiplying out we get:

$$\frac{d\vec{m}}{dt}=\gamma\,\vec{m}\times\vec{B}-\frac{\alpha\,\gamma}{|\vec{m}|}\vec{m}\times\vec{m}\times\vec{B}+\frac{\alpha^2}{|\vec{m}|^2}\vec{m}\times\vec{m}\times\frac{d\vec{m}}{dt}\qquad(3)$$

•Using vector identity $\vec{a}\times(\vec{b}\times\vec{c})=\vec{b}(\vec{a}\cdot\vec{c})-\vec{c}(\vec{a}\cdot\vec{b})$ we have:

$$\vec{m}\times\vec{m}\times\frac{d\vec{m}}{dt}=\vec{m}\left(\vec{m}\cdot\frac{d\vec{m}}{dt}\right)-\frac{d\vec{m}}{dt}|\vec{m}|^2$$

•Since the magnitude of ***m*** is assumed to be constant* there can be no component of $\frac{d\vec{m}}{dt}$ which is parallel to ***m***; we get then:

$$\vec{m}\times\vec{m}\times\frac{d\vec{m}}{dt}=-\frac{d\vec{m}}{dt}|\vec{m}|^2\qquad(4)$$

*if the system consists of a number of individual moments, each of which is damped slightly differently, the magnitude of the total magnetic moment may not be conserved; one should use Bloch equation then.

Landau-Lifshitz-Gilbert (LLG) equation of spin motion

- Inserting Eq. (4) into Eq. (3) we obtain:

$$\frac{d\vec{m}}{dt} = \gamma\,\vec{m}\times\vec{B} - \frac{\alpha\,\gamma}{|\vec{m}|}\vec{m}\times\vec{m}\times\vec{B} - \alpha^2\frac{d\vec{m}}{dt}$$

$$\alpha = \gamma\,\eta\,|\vec{m}|$$

$$\frac{d\vec{m}}{dt}(1+\alpha^2) = \gamma\,\vec{m}\times\vec{B} - \frac{\alpha\,\gamma}{|\vec{m}|}\vec{m}\times\vec{m}\times\vec{B}$$

- And finally:

Landau-Lifshitz-Gilbert equation

$$\boxed{\frac{d\vec{m}}{dt} = \frac{\gamma}{(1+\alpha^2)}\vec{m}\times\vec{B} - \frac{\alpha}{(1+\alpha^2)}\frac{\gamma}{|\vec{m}|}\vec{m}\times\vec{m}\times\vec{B}}$$

- In general the magnetic induction should be replaced by the effective field ***B***eff [9, p. 178]:

$$\vec{B}_{eff} = \mu_0\left(\frac{C}{M^2}\left[(\nabla M_x)^2+(\nabla M_y)^2+(\nabla M_z)^2\right] + \vec{H} + \frac{\partial}{\partial\vec{m}}E_{anisotropy}\right)$$

exchange energy density – see lecture no. 8

to be read as $\frac{\partial}{\partial\vec{m}}f = \hat{x}\frac{\partial}{\partial m_x}f + \hat{y}\frac{\partial}{\partial m_y}f + \hat{z}\frac{\partial}{\partial m_z}f$ [9, p.178]

Landau-Lifshitz-Gilbert (LLG) equation of spin motion

Landau-Lifshitz-Gilbert equation

$$\frac{d\vec{m}}{dt}=\frac{\gamma_G}{(1+\alpha_G^2)}\vec{m}\times\vec{B}-\frac{\alpha_G}{(1+\alpha_G^2)}\frac{\gamma_G}{|\vec{m}|}\vec{m}\times\vec{m}\times\vec{B}$$

Landau-Lifshitz equation

$$\frac{d\vec{m}}{dt}=\gamma_L\vec{m}\times\vec{B}-\frac{\alpha_L}{|\vec{m}|}(\vec{m}\times(\vec{m}\times\vec{B}))$$

•With the replacement $\gamma_L=\frac{\gamma_G}{1+\alpha_G^2}$, $\alpha_L=\frac{\alpha_G\gamma_G}{1+\alpha_G^2}$ both equations have similar form but...

the dependencies of precessional and relaxation terms on damping constant are quite different [8]:

•According to LL equation the relaxation becomes faster with increasing damping α_L (red dashed curve) which is counter intuitive.

•In case of LLG equation the behavior of both terms agree with the expectations for the dynamics of damped precession [8].

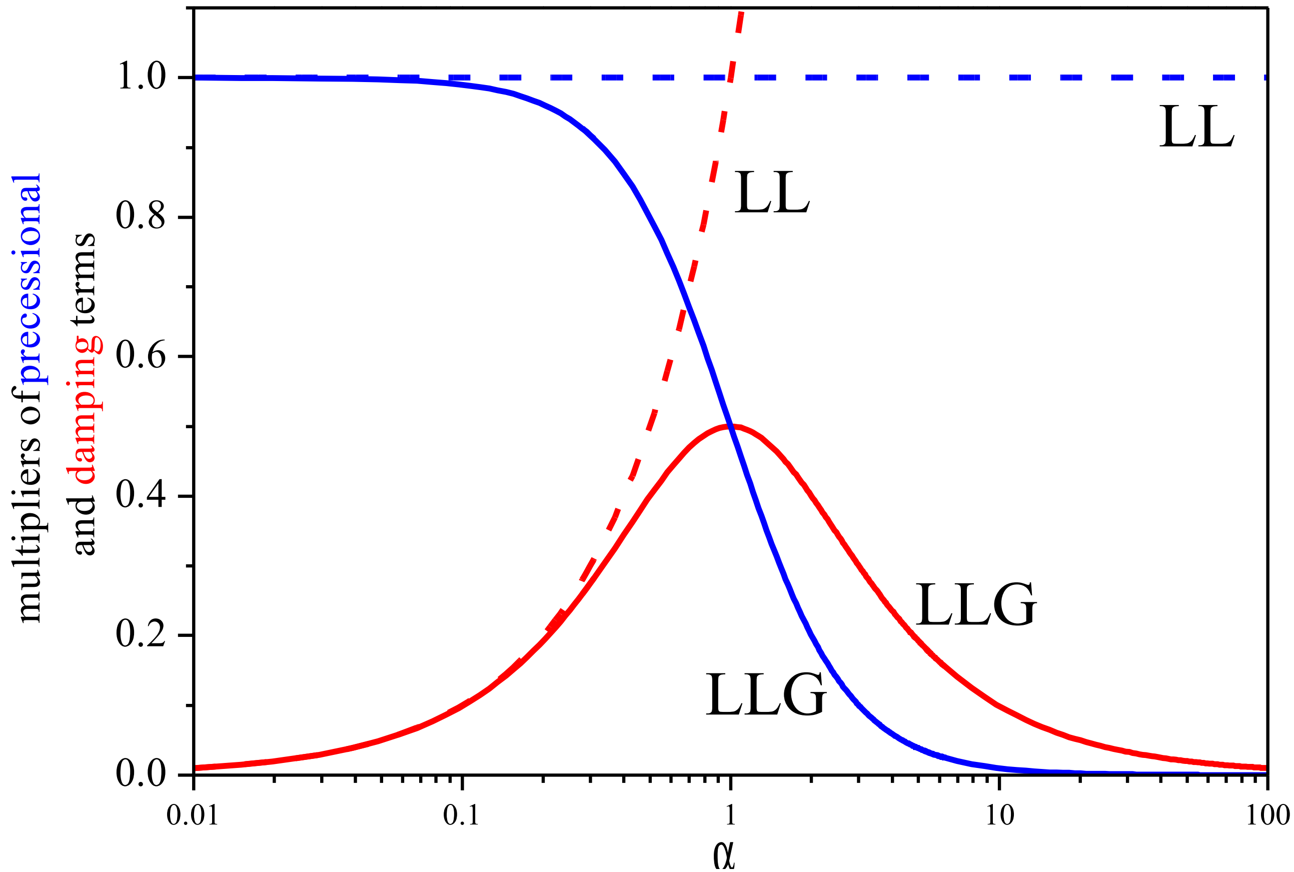

Magnetic moment reversal

- Let us consider the LLG equation describing the orientation of a single moment (monodomain state) of magnetized sphere fixed in space (no translational motion):

$$\frac{d\vec{M}}{dt}=\frac{\gamma\mu_0}{(1+\alpha^2)}\left(\vec{M}\times\vec{H}-\frac{\alpha}{M}\left[\vec{M}\times(\vec{M}\times\vec{H})\right]\right)$$

- For simplicity the time scale is changed: $\tau=\dfrac{tM\gamma\mu_0}{(1+a^2)}$

$$M^2\frac{d\vec{M}}{d\tau}=M\,\vec{M}\times\vec{H}-\alpha\left[\vec{M}\times(\vec{M}\times\vec{H})\right]$$

- We assume that the external field is applied along z-direction [$\mathbf{B}_a/\mu_0=(0,0,H_z)$]. The demagnetizing field inside the sphere is ($\mathbf{H}_d=-1/3\,\mathbf{M}$). With $\mathbf{H}=\mathbf{H}_a-\mathbf{H}_d$ we obtain:

$$M^2\frac{dM_x}{d\tau}=-\alpha H_z M_x M_z+H_z M_y M$$

$$M^2\frac{dM_y}{d\tau}=-\alpha H_z M_y M_z-H_z M_x M$$

$$M^2\frac{dM_z}{d\tau}=\alpha\left(H_z M_x^2+H_z M_y^2\right)$$

- Verifying that d***M*** is perpendicular to ***M*** [$(dM_x, dM_y, dM_z)\cdot\vec{M}=0$] we see that the length of the magnetization is preserved as expected.

Ryoichi Kikuchi, J. Appl. Phys. 27, 1352 (1956)

Magnetic moment reversal

- We can then rewrite the equation for M_z obtaining the equation of motion that does not depend on M_x and M_y:

$$M^2 \frac{dM_z}{d\tau} = \alpha H_z \left(M^2 - M_z^2 \right) \xleftarrow{|\vec{M}| = const} M^2 \frac{dM_z}{d\tau} = \alpha \left(H_z M_x^2 + H_z M_y^2 \right)$$

- Integrating between the final and the initial values of M_z we have:

$$\alpha H_z \tau = \int_{M_z^i}^{M_z^f} \frac{M^2}{\left(M^2 - M_z^2\right)} dM_z = M \; ArcTanh\left[\frac{M_z}{M}\right]_{M_z^i}^{M_z^f} = M \ln \left| \frac{\sqrt{-1 - M_z/M}}{\sqrt{-1 + M_z/M}} \right|_{M_z^i}^{M_z^f} =$$

$$M \left(\ln \left| \sqrt{\frac{-1 - M_z^f/M}{-1 + M_z^f/M}} \right| - \ln \left| \sqrt{\frac{-1 - M_z^i/M}{-1 + M_z^i/M}} \right| \right) = M \left(\ln \left| \sqrt{\frac{-1 - M_z^f/M}{-1 + M_z^f/M} \; \frac{-1 + M_z^i/M}{-1 - M_z^i/M}} \right| \right) =$$

$$\frac{1}{2} M \ln \left| \frac{\left(M + M_z^f\right)\left(M - M_z^i\right)}{\left(M - M_z^f\right)\left(M + M_z^i\right)} \right|$$

- Going back to the actual time we get for the time for M_z to change from the initial to final value:

$$\tau = \frac{t M \gamma \mu_0}{\left(1 + a^2\right)}$$

$$\boxed{t_F = \frac{1}{2 \gamma H_z} \frac{1 + \alpha^2}{\alpha} \ln \left| \frac{\left(M + M_z^f\right)\left(M - M_z^i\right)}{\left(M - M_z^f\right)\left(M + M_z^i\right)} \right|}$$

Ryoichi Kikuchi, J. Appl. Phys. 27, 1352 (1956)

Magnetic moment reversal

$$t_F = \frac{1}{2\gamma H_z}\frac{1+\alpha^2}{\alpha}\ln\left|\frac{(M+M_z^f)(M-M_z^i)}{(M-M_z^f)(M+M_z^i)}\right|$$

- If at t=0 the magnetization/moment points exactly along z-axis (M_Z=-M) then t_F would be infinite – **no switching**.
- If there is no damping (α=0) then t_F would be infinite – the moment of the sample would precess around the external field direction.

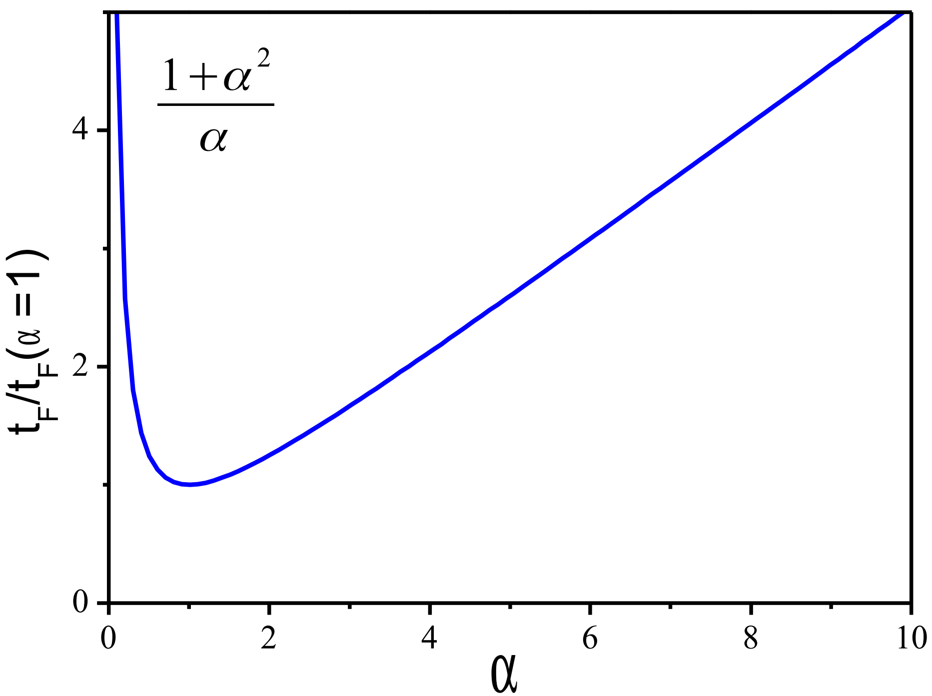

- The shortest switching time is obtained for finite value of damping coefficient (α=1).
- The value of the critical damping constant depends on the shape of the sample.
- For single domain thin film the critical α is about 0.013.
- For permalloy films the minimum switching time, as obtained from the similar calculations is about **1 ns**.

Ryoichi Kikuchi, J. Appl. Phys. 27, 1352 (1956)

Magnetic moment reversal

- Time evolution of magnetic moment orientation for low and high damping:
  - initial orientation of magnetic moment: (0,0.001,1)
  - magnetic field instantaneously switched on to value: (0,0,-1)

H∥***z*** axis

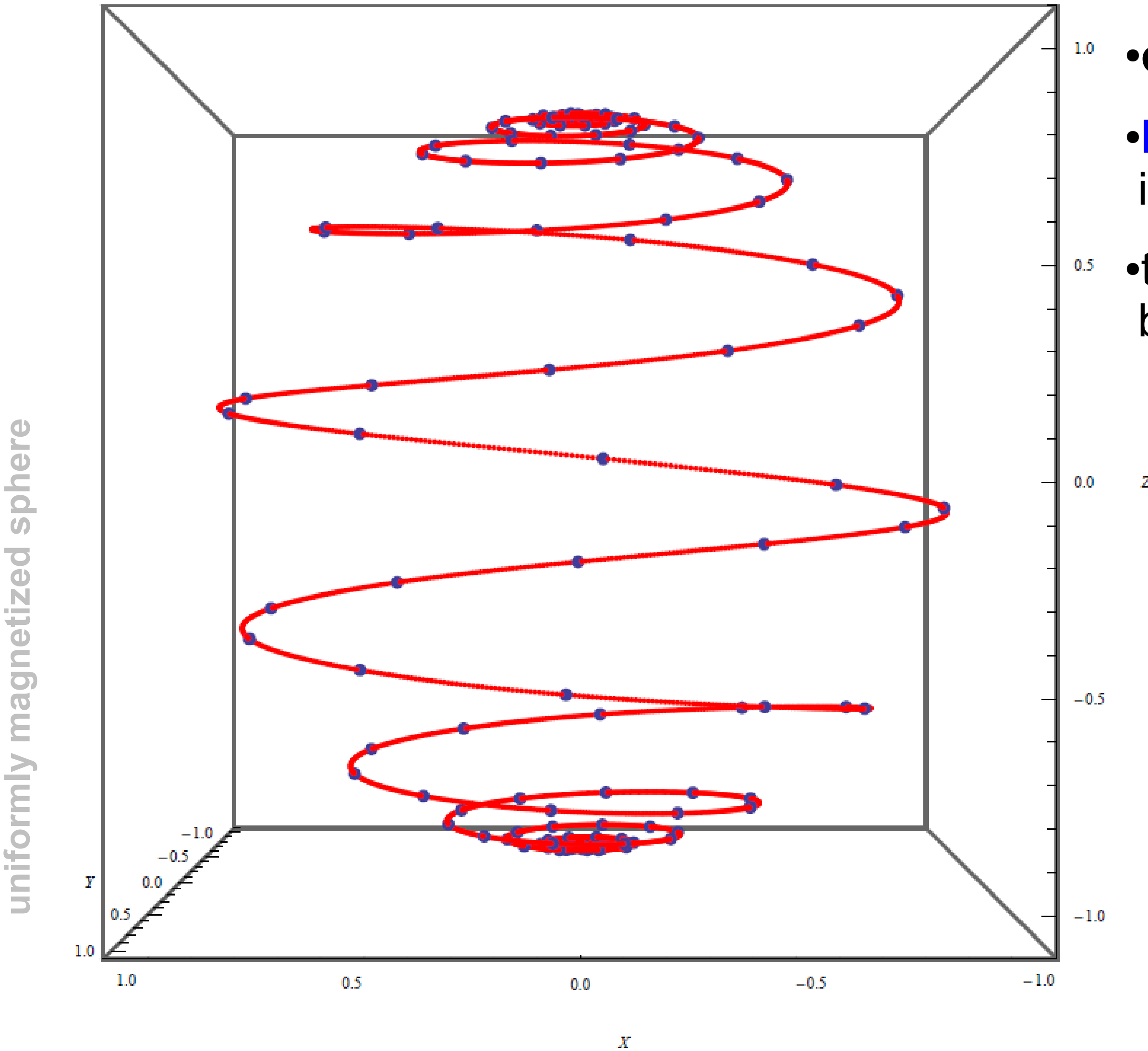

- **α=0.1**
- **blue dots** mark the same time intervals
- the end of moment moves from top to bottom

Wolfram Mathematica 6.0 code to obtain these curves:

```
ilepunktow=9000;
orientacjamomentu=Table[{0,0,0},{i,1,ilepunktow-1}];
dt=0.025;
alfa=0.1;
Hz=-1;
Mi={0,0.001,1};(*initial moment orientation*)
moment=Sqrt[Mi.Mi];(*moment's length*)
licznik=0;
gamma=2;
timemultiplier=1/(moment gamma (1+alfa^2));

coile=50;(*co ile punktow stawiac marker*)
macierzznacznikow=Table[{0,0,0},{i,1,Floor[ilepunktow/coile]-1}];
licznik=1;
l=1;
For[k=1,k<ilepunktow,k++,

Mi[[1]]=Mi[[1]]+dt timemultiplier  Hz(moment Mi[[2]] -alfa Mi[[1]] Mi[[3]])/moment^2;
Mi[[2]]=Mi[[2]]+dt timemultiplier  Hz(-moment Mi[[1]] -alfa Mi[[2]] Mi[[3]])/moment^2;
Mi[[3]]=Mi[[3]]+dt timemultiplier Hz alfa (Mi[[1]]^2+ Mi[[2]]^2)/moment^2;
orientacjamomentu[[k,1]]=Mi[[1]];orientacjamomentu[[k,2]]=Mi[[2]];orientacjamomentu[[k,3]]=Mi[[3]];

(*matrix of markers*)
If[licznik<coile,licznik=licznik+1,{licznik=1;
macierzznacznikow[[l,1]]=orientacjamomentu[[k,1]];
macierzznacznikow[[l,2]]=orientacjamomentu[[k,2]];
macierzznacznikow[[l,3]]=orientacjamomentu[[k,3]];

l++}
]

]
wy1=ListPointPlot3D[orientacjamomentu, PlotRange->{{-1.1,1.1},{-1.1,1.1},{-1.1,1.1}},
BoxRatios->{1,1,1},PlotStyle->{Red},AxesLabel->{X,Y,Z},ViewPoint->{0,Pi,0},BoxStyle->Directive[Thickness[0.004]]];

wy4=ListPointPlot3D[macierzznacznikow, PlotRange->{{-1.1,1.1},{-1.1,1.1},{-1.1,1.1}},
BoxRatios->{1,1,1},PlotStyle->PointSize[Large],AxesLabel->{X,Y,Z},ImageSize->600,ViewPoint->{Pi,Pi/2,2}];
wy2=Graphics3D[{Opacity[0.5],Sphere[{0,0,0},1]}];
wy3=Graphics3D[{AbsoluteThickness[2],Line[{{0,0,0},{0,0,1}}]}];
wy3=Show[wy1,wy2,wy3,wy4,ImageSize->600,ViewPoint->{Pi,Pi/2,2},ImageMargins->20]
```

Ryoichi Kikuchi, J. Appl. Phys. 27, 1352 (1956)

Magnetic moment reversal

- Time evolution of magnetic moment orientation for low and high damping:
  - initial orientation of magnetic moment: (0,0.001,1)
  - magnetic field instantaneously switched on to value: (0,0,-1)

H∦***z*** axis

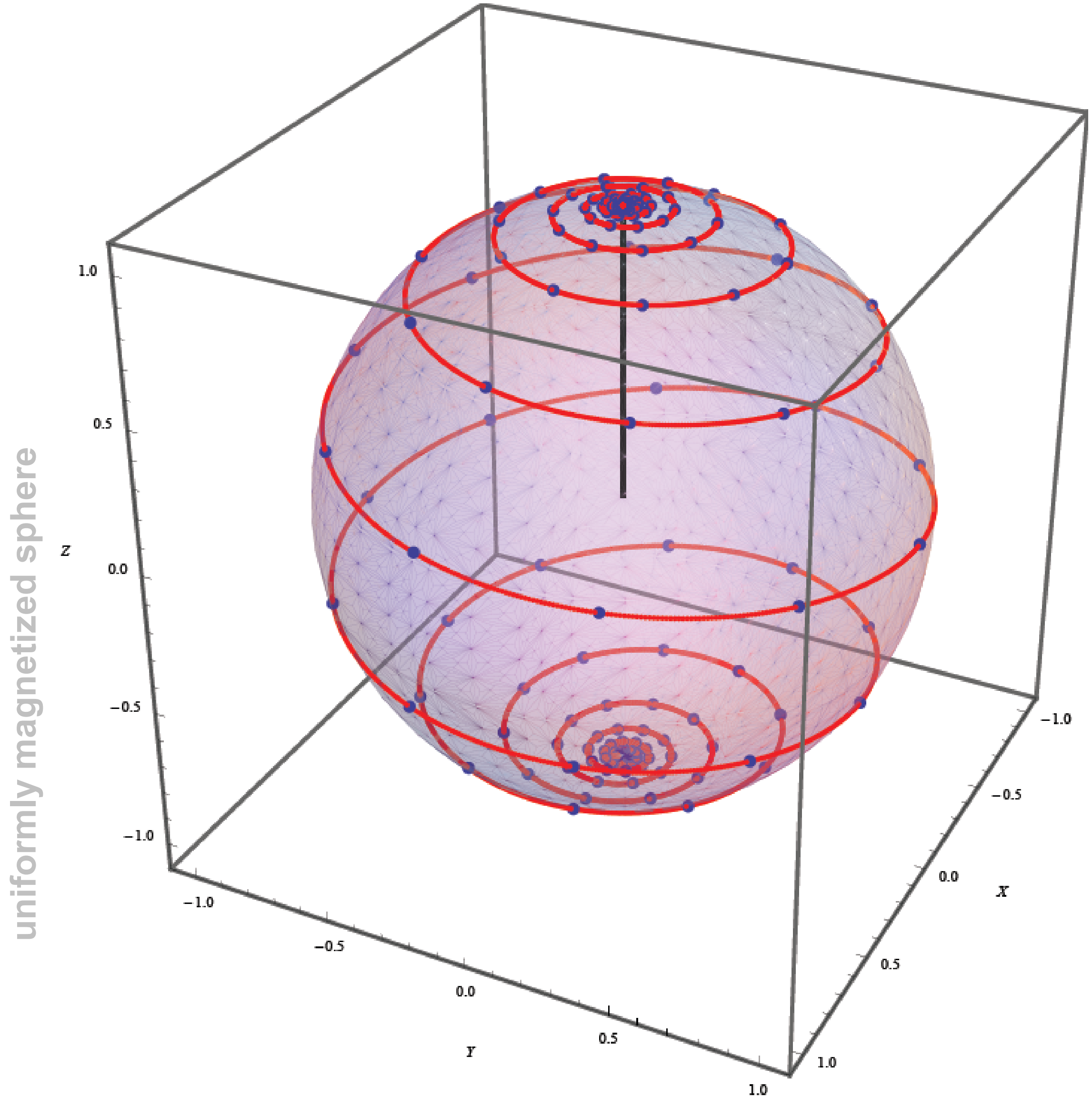

- **α=0.1**
- **blue dots** mark the same time intervals
- the end of moment moves from top to bottom

Ryoichi Kikuchi, J. Appl. Phys. 27, 1352 (1956)

Magnetic moment reversal

•Time evolution of magnetic moment orientation for low and high damping:

➢initial orientation of magnetic moment: (0,0.001,1)

➢magnetic field instantaneously switched on to value: (0,0,-1)

H∦***z*** axis

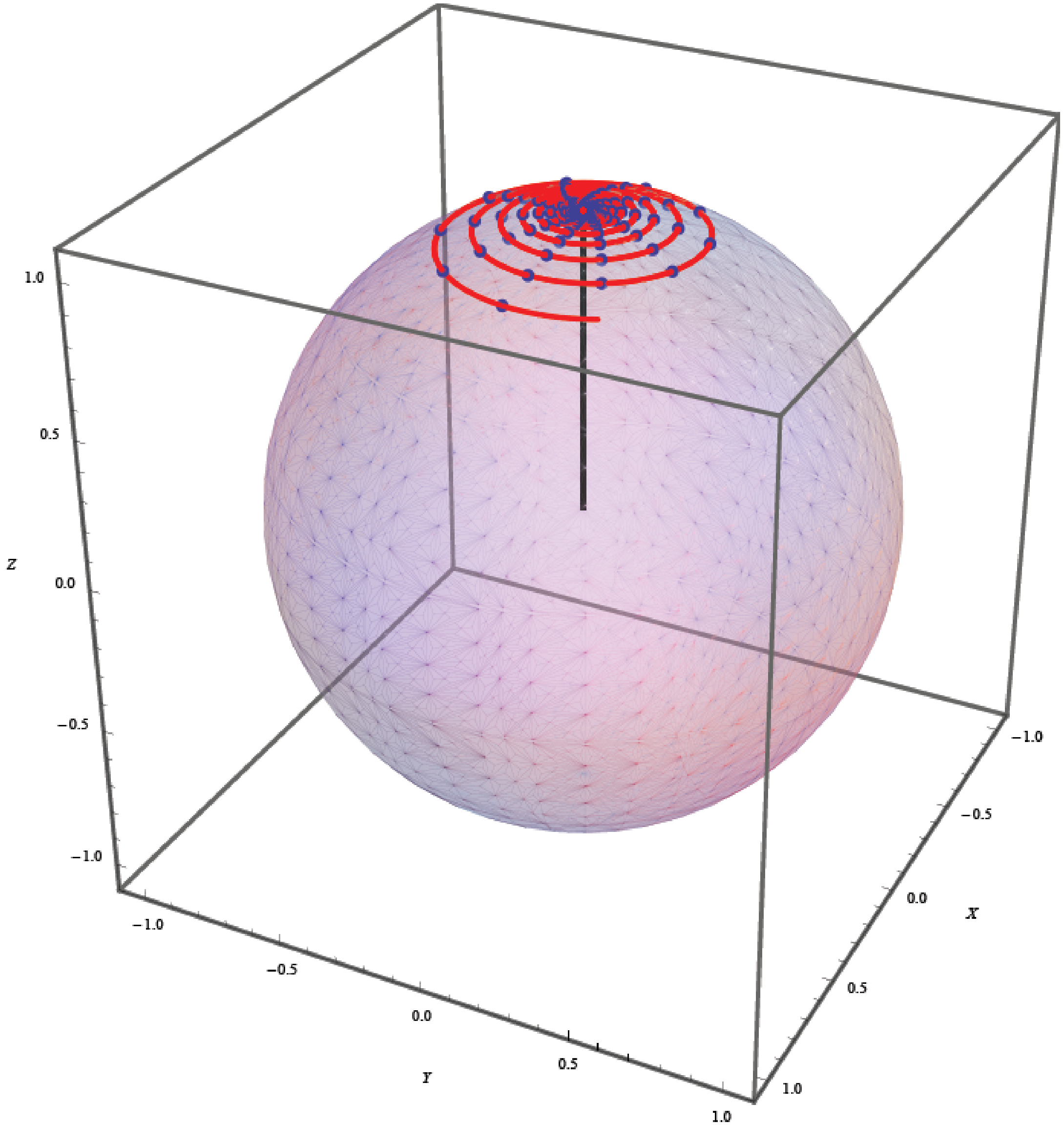

uniformly magnetized sphere

•**α=0.05**

•**blue dots** mark the same time intervals

•the end of moment moves from top to bottom

•the total time of movement is the same as on the previous page

•note that due to weaker damping the moment did not change its orientation to -*z* – **the switching is delayed**

Ryoichi Kikuchi, J. Appl. Phys. 27, 1352 (1956)

Magnetic moment reversal

- Time evolution of magnetic moment orientation for low and high damping:
  - initial orientation of magnetic moment: (0,0.001,1)
  - magnetic field instantaneously switched on to value: (0,0,-1)

H∥***z*** axis

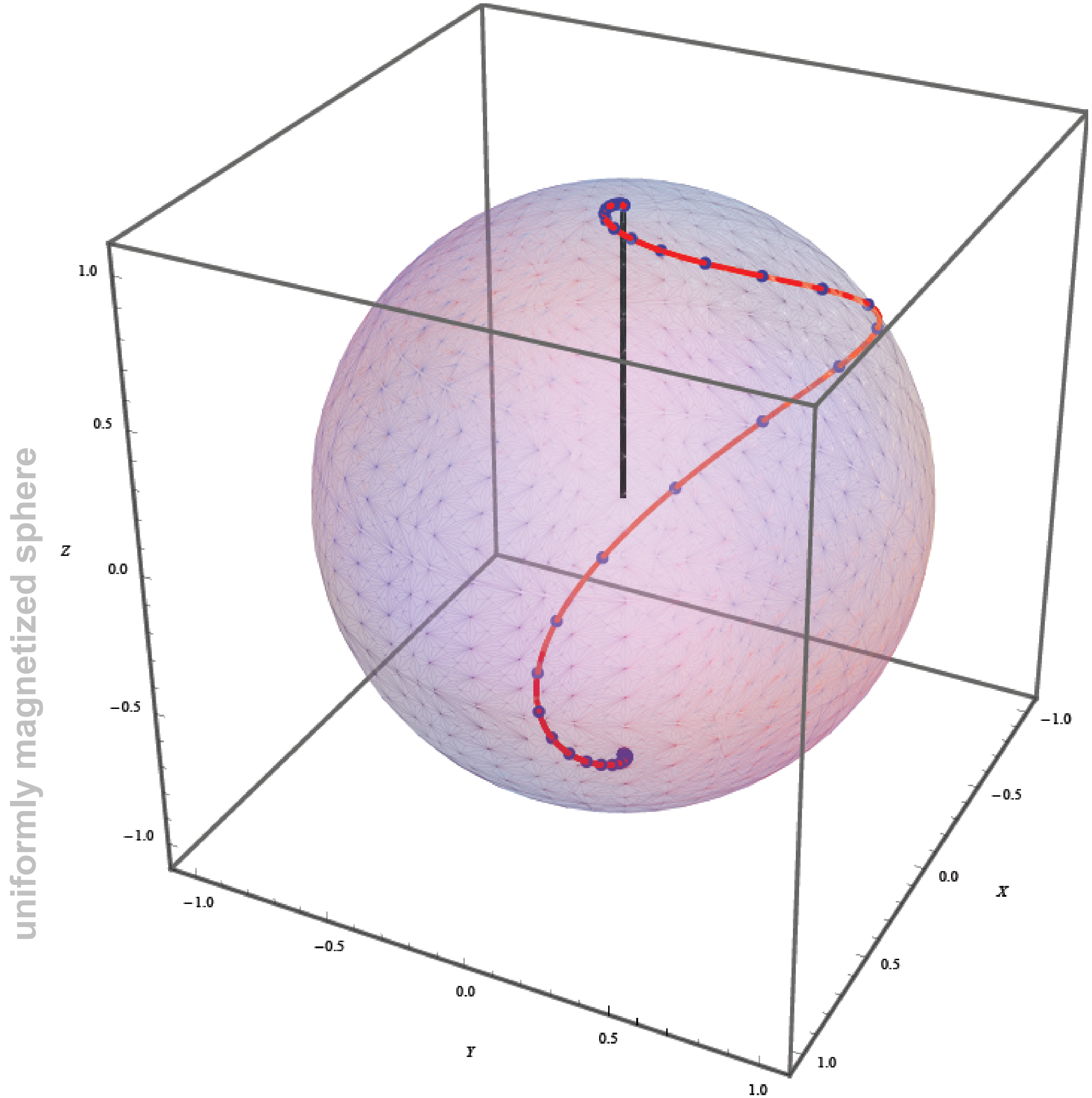

- **α=1** – **minimal switching time**
- **blue dots** mark the same time intervals
- the end of moment moves from top to bottom

Ryoichi Kikuchi, J. Appl. Phys. 27, 1352 (1956)

Magnetic moment reversal

- Note that further increase of damping constant α slows down the switching of magnetic moment (more blue dots)

- **α=1** – **minimal switching time**

uniformly magnetized sphere

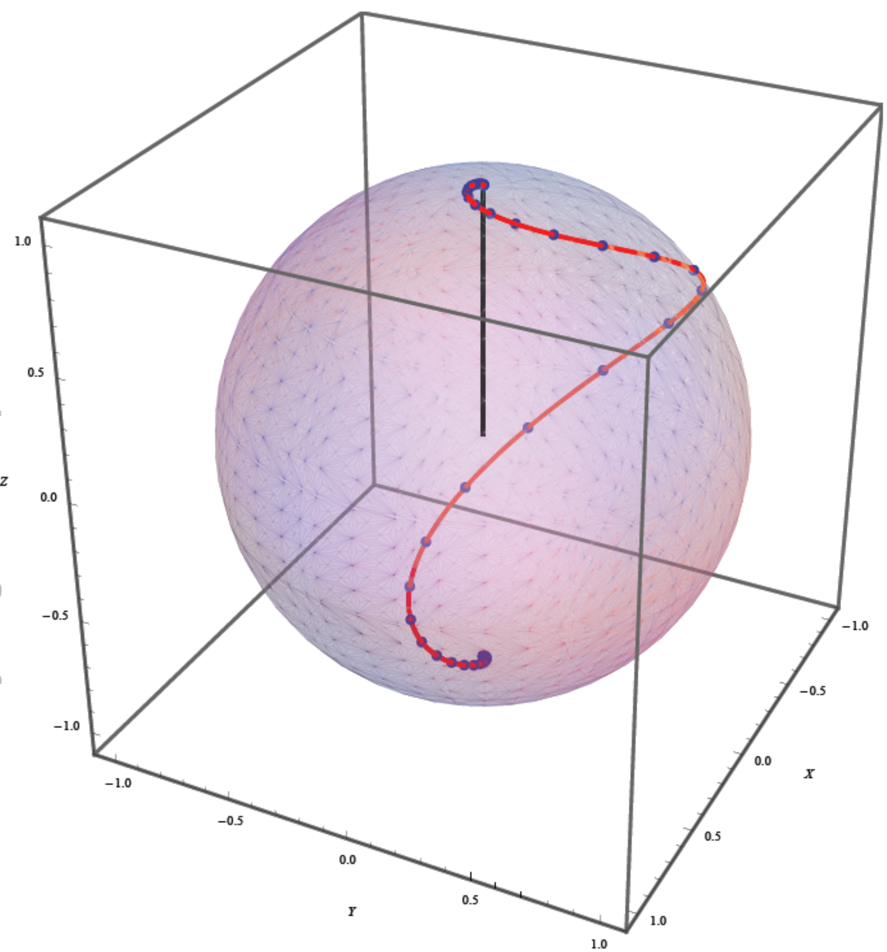

- **α=10**

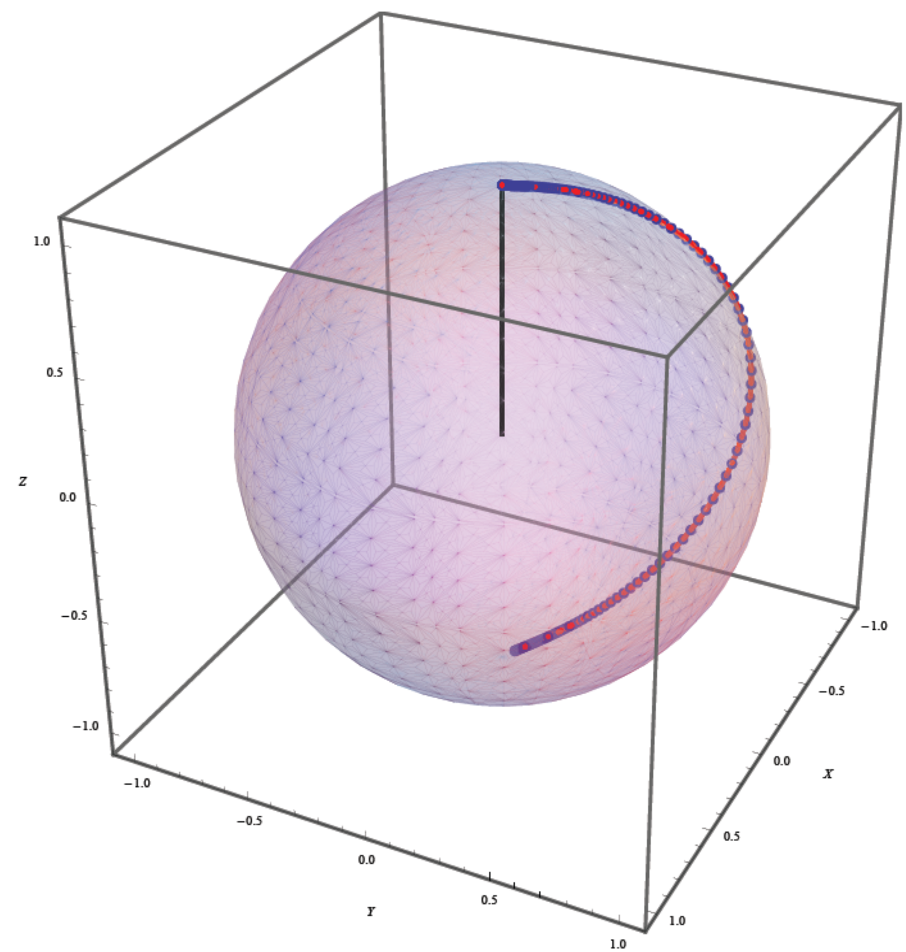

Ryoichi Kikuchi, J. Appl. Phys. 27, 1352 (1956)

Magnetic moment reversal – thin film

•Time evolution of magnetic moment orientation for low and high damping:
➢initial orientation of magnetic moment: (-1,0.001,0) – in plane of the sample
➢magnetic field instantaneously switched on to value: (+1,0,0)

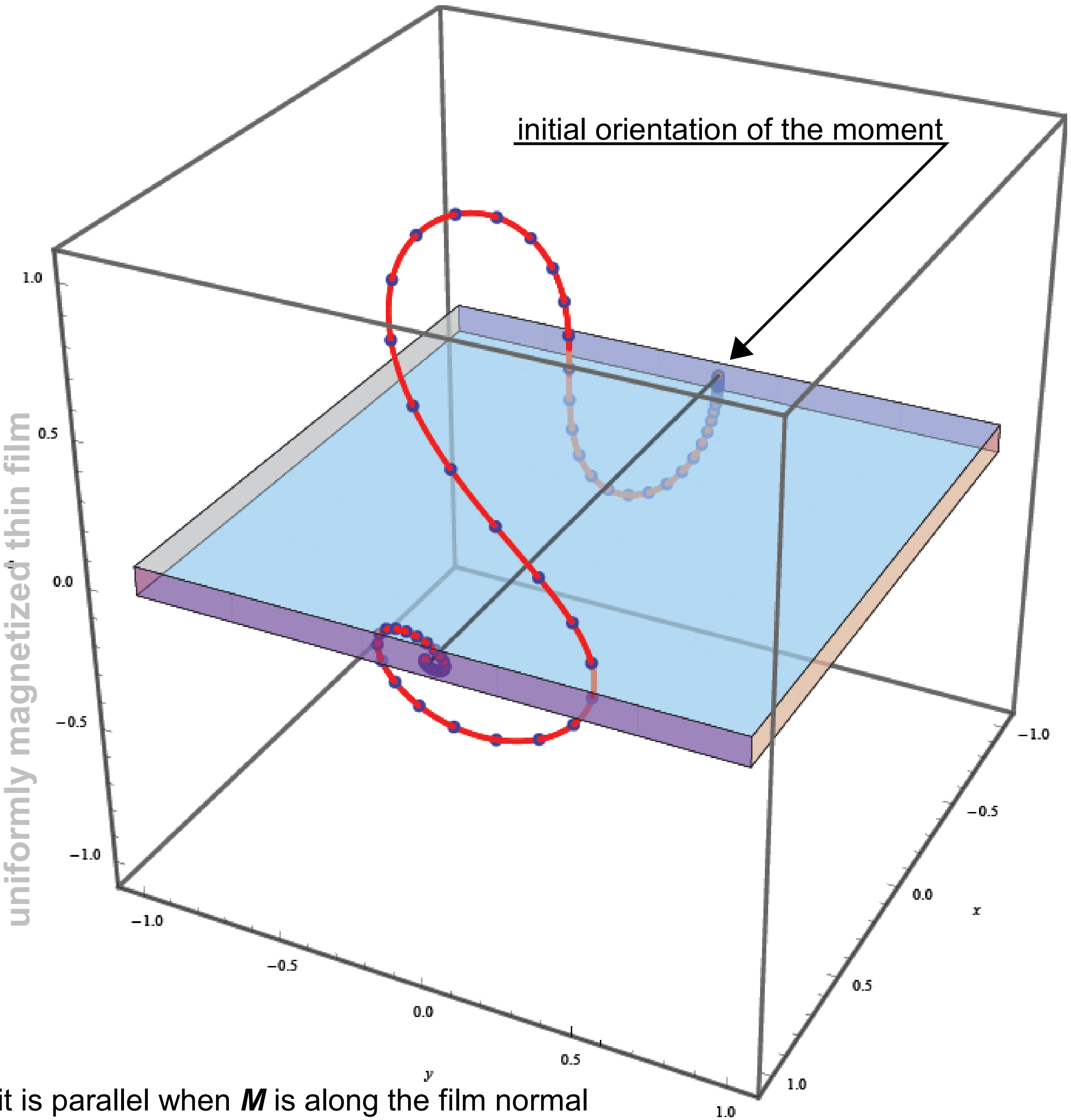

•**α=0**

•the end of moment moves from behind to the front

•**blue dots** mark the same time intervals

•in thin films, contrary to the case of the single domain sphere, the demagnetizing field is, in general*, not parallel to magnetic moment and exerts a torque on it $\Longrightarrow$ the switching time depends on the magnetization

•for large α:

$$t_F \propto \frac{\alpha}{M}$$

$$\vec{H}_{demag} = -\hat{z} M_z$$

*it is parallel when ***M*** is along the film normal

Ryoichi Kikuchi, J. Appl. Phys. 27, 1352 (1956)

Magnetic moment reversal – thin film

- Time evolution of magnetic moment orientation for low and high damping:
  - initial orientation of magnetic moment: (-1,0.001,0) – in plane of the sample
  - magnetic field instantaneously switched on to value: (+1,0,0)

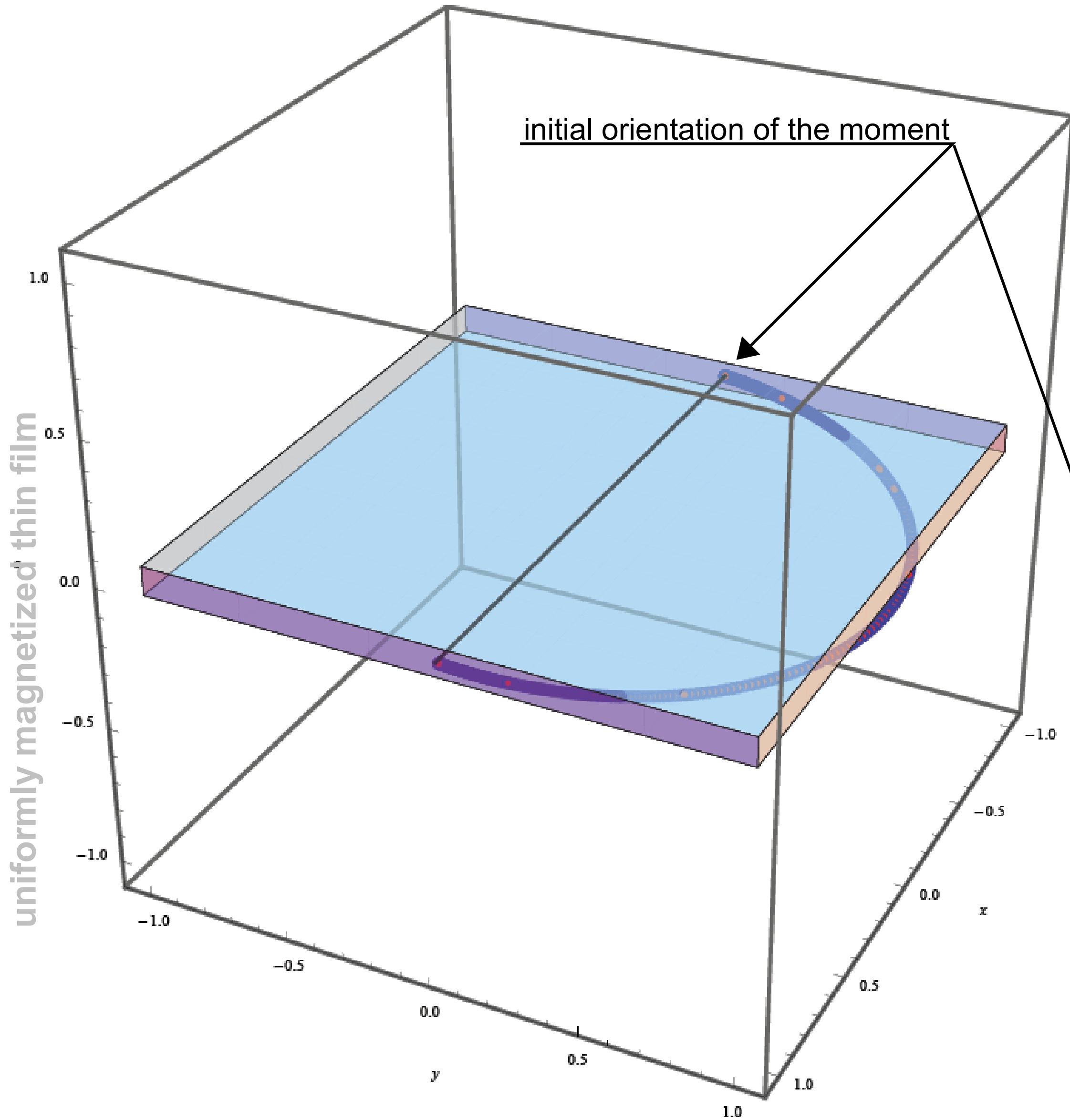

- **α=10**
- the end of moment moves from behind to the front
- If damping is high the moment rotates almost within **xy plane** and approaches field directions monotonically without oscillations

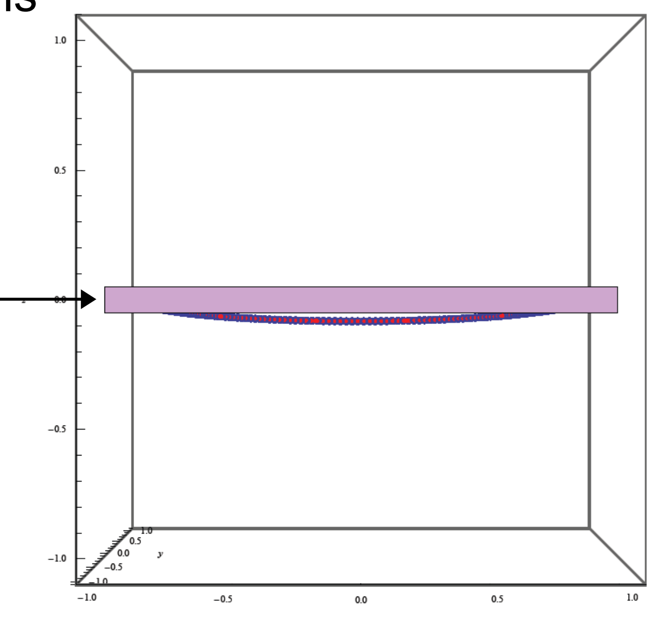

Ryoichi Kikuchi, J. Appl. Phys. 27, 1352 (1956)

Magnetic moment reversal – approach to saturation

- Trajectory of the moment depends on the field value:
  - initial orientation of magnetic moment: (-1,0.001,0) – in plane of the sample
  - magnetic field instantaneously switched on to value: (+1,0,0) (red line) or (**+3**,0,0) (**green** line)

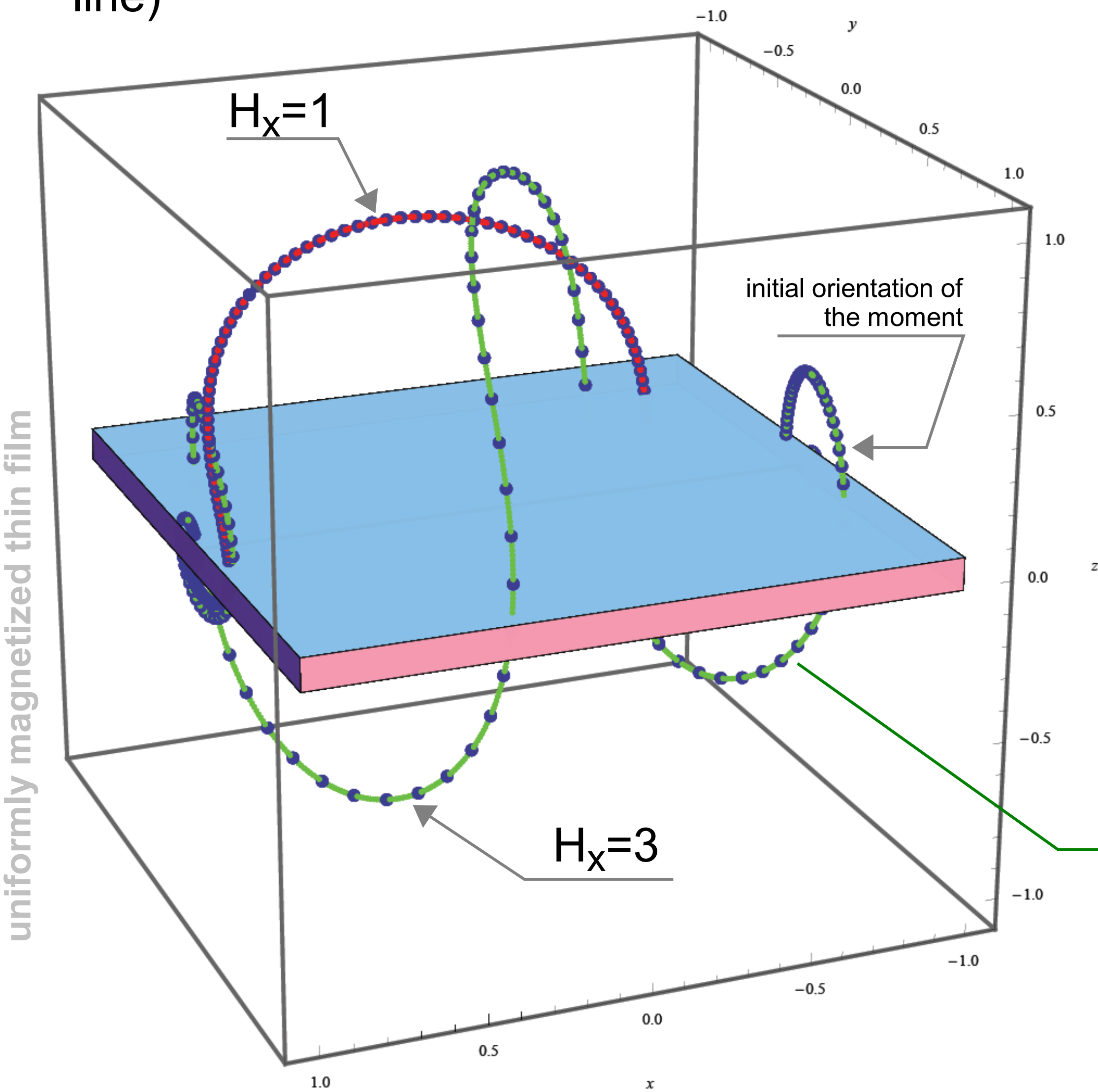

- **α=0.009**
- the component of magnetization parallel to the external field oscillatorilly approaches saturation

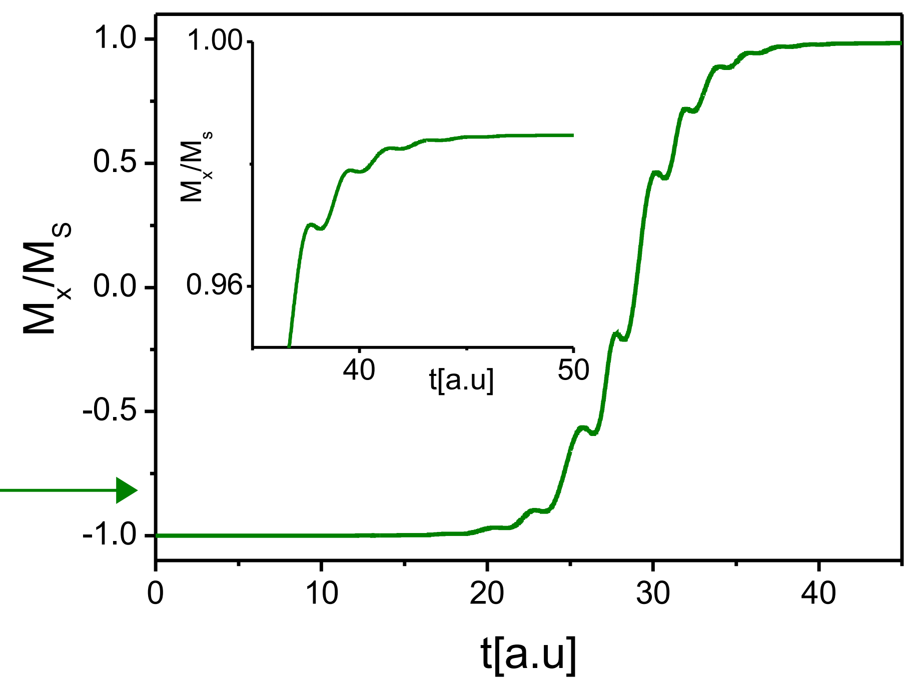

blue dots mark the same time intervals

Ryoichi Kikuchi, J. Appl. Phys. 27, 1352 (1956)

Element-resolved precessional dynamics

- Sputtered, 0.35 mm wide Cu(75nm)/Py(25nm)/Cu(3nm) trilayer
- Current pulses through thick Cu layer (10ns duration) create field pulses (Oersted field) perpendicular to the film stripline* (in plane of the film)
- A bias field $\boldsymbol{H}_b$ can be applied parallel to the stripline in order to align the initial magnetization prior to excitation.
- **Element-selective** x-ray resonant magnetic scattering (XRMS)

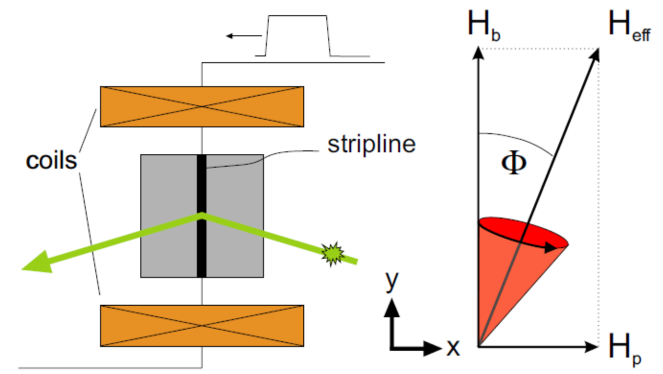

Figure 1. Schematic of the setup and fields applied at the sample region. The 350 μm stripline is centred on a Si substrate and oriented perpendicular to the scattering plane. A pair of coils provides the bias field H_b along the y-axis, the pulse field from the stripline is parallel to the x-axis. With our setup the change in the M_x-component is measured while the magnetization precesses around the effective field direction H_{eff}.

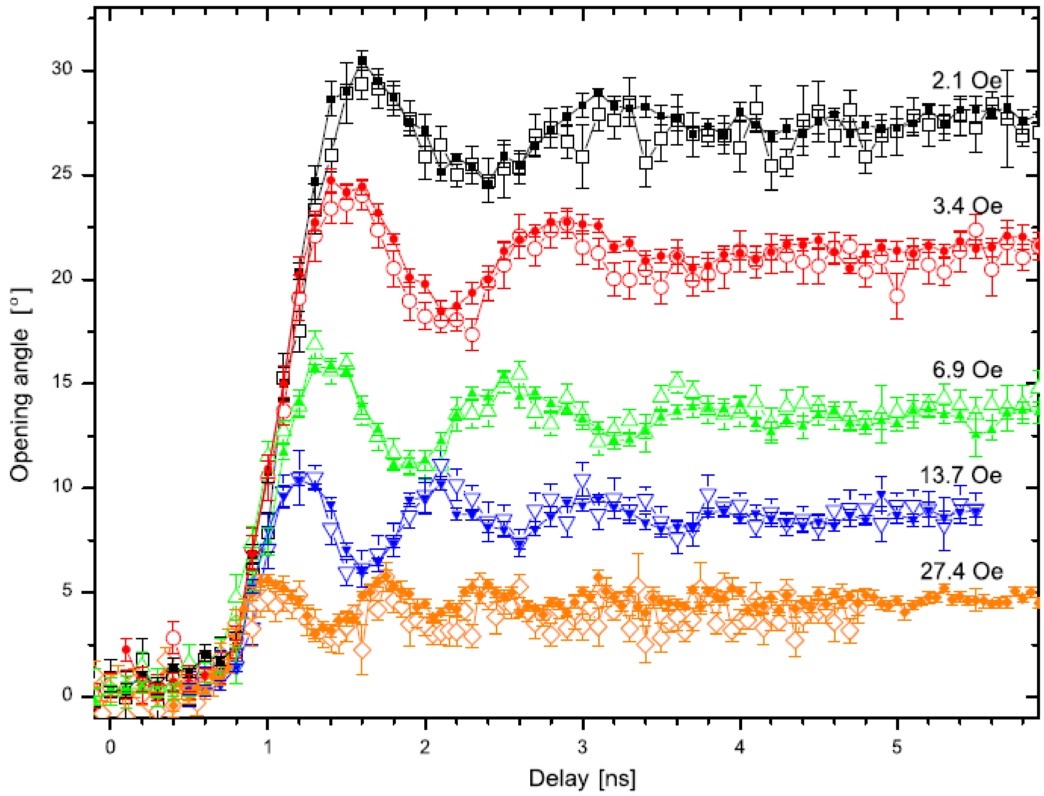

authors' "data show that Fe and Ni moments are aligned parallel to each other at all times, while they oscillate around the effective field direction given by the step field pulse and applied bias field"

Figure **5**. Comparison of the magnetization dynamics measured at the **Fe** (full) and **Ni** (open symbols) resonant edges for a set of different bias fields. The detected intensity is converted into opening angle φ according to the hysteresis curves.

S. Buschhorn, F. Brüssing, R. Abrudan and H. Zabel, J. Phys. D: Appl. Phys. **44** ,165001 (2011)

*for the field of the current sheet see lecture 2

Bibliography:

[1] A. Hubert, R. Schäfer, Magnetic domains: the analysis of magnetic microstructures, Springer 1998
[2] P. Суху, Магнитные Тонкие Пленки, Издательство МИР Москва 1967
[3] W. Ketterle, MIT Physics 8.421 Atomic and optical Physics, http://cua.mit.edu/8.421_S06/
[4] M. Getzlaff, Fundamentals of Magnetism, Springer-Verlag Berlin-Heidelberg 2008
[5] H. Kronümller, General Micromagnetic Theory, in Handbook of Magnetism and Advanced Magnetic Materials, edited by H. Kronümller and S.S.P. Parkin, vol. 2, Wiley, 2007.
[6] T. Gilbert, IEEE Trans. Magn. **40**, 3443 (2004)
[7] J. Miltat and M. Donahue, Numerical micromagnetics: finite difference methods, in Handbook of Magnetism and Advanced Magnetic Materials, edited by H. Kronümller and S.S.P. Parkin, vol. 2, Wiley, 2007.
[8] H. Kronmüller, M. Fähnle, Micromagnetism and the Microstructure of Ferromagnetic Solids, Cambridge University Press, 2003
[9] A. Aharoni, Introduction to the Theory of Ferromagnetism, Clarendon Press, Oxford 1996